Multiple- and Single-Molecule Analysis of the Actomyosin Motor by Nanometer-Piconewton Manipulation with a Microneedle: Unitary Steps and Forces

Akihiko Ishijima,*‡ Hiroaki Kojima,* Hideo Higuchi,* Yoshie Harada,* Takashi Funatsu,* and Toshio Yanagida*§
*Bio-Motron Project, ERATO, JRDC, Mino, Osaka, ‡Wako Research Center, HONDA R&D Co. Ltd, Wako, Saitama, and §Department of Biophysical Engineering, Osaka University, Toyonaka, Osaka, Japan

ABSTRACT We have developed a new technique for measurements of piconewton forces and nanometer displacements in the millisecond time range caused by actin-myosin interaction in vitro by manipulating single actin filaments with a glass microneedle. Here, we describe in full the details of this method. Using this method, the elementary events in energy transduction by the actomyosin motor, driven by ATP hydrolysis, were directly recorded from multiple and single molecules. We found that not only the velocity but also the force greatly depended on the orientations of myosin relative to the actin filament axis. Therefore, to avoid the effects of random orientation of myosin and association of myosin with an artificial substrate in the surface motility assay, we measured forces and displacements by myosin molecules correctly oriented in single synthetic myosin rod cofilaments. At a high myosin-to-rod ratio, large force fluctuations were observed when the actin filament interacted in the correct orientation with a cofilament. The noise analysis of the force fluctuations caused by a small number of heads showed that the myosin head generated a force of 5.9 ± 0.8 pN at peak and 2.1 ± 0.4 pN on average over the whole ATPase cycle. The rate constants for transitions into (k_+) and out of (k_-) the force generation state and the duty ratio were 12 ± 2 s^{-1}, and 22 ± 4 s^{-1}, and 0.36 ± 0.07, respectively. The stiffness was 0.14 pN nm^{-1} $head^{-1}$ for slow length change (100 Hz), which would be approximately 0.28 pN nm^{-1} $head^{-1}$ for rapid length change or in rigor. At a very low myosin-to-rod ratio, distinct actomyosin attachment, force generation (the power stroke), and detachment events were directly detected. At high load, one power stroke generated a force spike with a peak value of 5–6 pN and a duration of 50 ms (k_-^{-1}), which were compatible with those of individual myosin heads deduced from the force fluctuations. As the load was reduced, the force of the power stroke decreased and the needle displacement increased. At near zero load, the mean size of single displacement spikes, i.e., the unitary steps caused by correctly oriented myosin, which were corrected for the stiffness of the needle-to-myosin linkage and the randomizing effect by the thermal vibration of the needle, was approximately 20 nm.

INTRODUCTION

Investigations of actomyosin, the motor protein of muscle and many nonmuscle cells, have recently made rapid progress. This is due in large part to application of in vitro motility assays that address the elementary processes directly at the molecular level (Huxley, 1990). An assay in wide use allows us to observe single fluorescent labeled actin filaments by optical microscopy (Yanagida et al., 1984) as well as the movements of actin produced by myosin or its subfragments bound to an artificial substrate (Kron and Spudich, 1986; Toyoshima et al., 1987; Harada et al., 1987). These assays have provided a great deal of insight into the relationship between the structure and functions of myosin (Harada et al., 1987; Toyoshima et al., 1987; Lowey et al., 1993; Itakura et al., 1993) and actin (Sutoh et al., 1991; Johara et al., 1993; Nishizaka et al., 1993; Prochniewicz and Yanagida, 1990) and the coupling between the ATPase and mechanical events (Harada et al., 1990; Toyoshima et al., 1990; Uyeda et al., 1990, 1991; Saitoh et al., 1994). Furthermore, we have developed a new technique for manipulating a single actin filament by a very fine glass needle to measure and exert the force on it (Kishino and Yanagida, 1988). This technique has been recently extended to measure displacements and forces with nanometer and piconewton resolutions, respectively, in the millisecond time range (Ishijima et al., 1991). Alternatively, a laser trap has been used for manipulating an actin filament attached to small particles to measure displacements and forces exerted on it, combined with nanometer measurements of the particle's position (Simmons et al., 1993; Finer et al., 1994; Miyata et al., 1994; Molloy et al., 1995a). The resolutions of these measurement systems are high enough to probe the force-generating process of individual myosin molecules interacting with actin. Recently these systems have allowed force and displacement to be measured directly from single myosin heads (Ishijima et al., 1994; Finer et al., 1994).

Here, we describe in full the details of a method for measurements of nanometer displacements and piconewton forces caused by actin-myosin interaction in vitro with millisecond resolution by manipulating single actin filaments with a glass microneedle. Using this method, we measured the force and displacement produced by both

Received for publication 9 December 1994 and in final form 27 September 1995.

Address reprint requests to Dr. Akihiko Ishijima, Bio-Motron Project, ERATO, JRDC, Senba-Higashi 2–4-14, Mino, Osaka, Japan. Tel.: 81-727-28-7003; Fax: 81-727-28-7033; E-mail: ishijima@yanagida.jrdc.go.jp.

0006-3495/96/01/383/18 $2.00

multiple and single myosin heads in synthetic myosin filaments interacting in the correct orientation with the actin filament. In the previous in vitro surface assays, myosin molecules or subfragments were randomly bound to artificial surfaces. Recent studies with the random myosin-coated surface replaced by intact and synthetic myosin filaments, however, have shown that the sliding velocity of actin toward the center of a filament (the forward direction, i.e., the normal physiological direction) is much greater than that in the opposite direction (away from the center) (Sellers and Kachar, 1990; Yamada et al., 1990; Ishijima and Yanagida, 1991; Yanagida, 1993; Yamada and Wakabayashi, 1993). These results suggest that the sliding force depends strongly on the orientation of the myosin molecules relative to the actin filament's polarity. The results obtained using the surface assay have not been entirely consistent. The reported velocities of myosin-induced actin filament movement have varied considerably (see Higashi-Fujime, 1991, for review), and the actin filament sliding distance produced by a single turnover of the ATPase reaction, termed the myosin step size, has been particularly controversial (Harada et al., 1990; Toyoshima et al., 1990; Uyeda et al., 1990, 1991; Ishijima et al., 1991; Huxley, 1990; Burton, 1992, for reviews). This variation is probably due mostly to the effects of the random orientation of myosin on the surface and the association of myosin with an artificial substrate (Yanagida, 1993). Therefore, it would be essential for quantitative analyses of experimental data to measure movements and force caused by myosin molecules with correct orientation and the functional domain being little affected by interaction with the surface. For this purpose, we used long synthetic myosin rod cofilaments, in which myosin molecules were regularly oriented and the heads were not directly attached to the surface. Using this system, sliding velocity and force as large as in muscle were reproduced in vitro.

Force fluctuations were measured when an actin filament interacted in the forward direction with a small number of myosin heads on a cofilament. Large fluctuations were observed at high load as in the surface assay (Ishijima et al., 1991), but the kinetic characteristics deduced from the noise analysis were different. In particular, the force of individual myosin heads was several times larger. As the density of myosin heads on the cofilament was greatly decreased, we recorded sharp force and displacement spikes at various loads. At high load, the force spikes were compatible with the molecular characteristics deduced from force fluctuations. In the field of membrane biophysics, fluctuations caused by gating of multiple channels also allows prediction of single channel properties (Katz and Miledi, 1971; Neher and Sackmann, 1976). Thus, we could determine the kinetic characteristics of myosin molecules by measuring force fluctuations from multiple molecules as well as by directly measuring force from single molecules, using the nanometer-piconewton manipulation technique.

Preliminary results have been published elsewhere (Ishijima et al., 1994).

MATERIALS AND METHODS

Protein preparation

Myosin and actin were obtained from rabbit skeletal muscle and purified as described previously (Harada et al., 1990). Heavy meromyosin (HMM) was obtained by α-chymotryptic digestion of myosin as described by Weeds and Pope (1977). Myosin rods were prepared and purified from rabbit skeletal myosin (Margossian and Lowey, 1982). Concentration of actin, myosin, myosin rod, and HMM were determined by using molar extinction coefficients of 1% protein solutions: for actin, $A_{290} = 0.63\ cm^{-1}$ and $M_r = 43{,}000$; for myosin, $A_{280} = 5.3\ cm^{-1}$, $M_r = 470{,}000$; for myosin rod, $A_{280} = 2.2\ cm^{-1}$, $M_r = 220{,}000$; for HMM, $A_{280} = 0.60\ cm^{-1}$, $M_r = 350{,}000$ (Margossian and Lowey, 1982). Myosin, myosin rod, and HMM were rapidly frozen in liquid nitrogen and stored at $-80°C$. Intact thick filaments were prepared from clam adductor muscle according to the method of Nonomura (1974).

Labeling proteins with fluorescent dyes

Actin filaments were labeled with phalloidin-tetramethylrhodamine isothiocyanate (PHD-TRITC; Molecular Probes, Eugene, OR) by incubating them (2.5 μM in actin monomers) in a solution containing 5 μM PHD-TRITC, 100 mM KCl, 10 mM HEPES (pH 7.0) overnight at 4°C (Harada et al., 1990). Labeling of myosin rods with fluorescein isothiocyanate (FITC; Molecular Probes) or TRITC (Molecular Probes) was started by adding the dyes dissolved in *N,N*-dimethylformamide (>10 mM) to myosin rod (~10 μM) in 0.6 M KCl, 10 mM HEPES, pH 7.0, at a dye-to-myosin molar ratio of 10:1. After incubation for 2 h at room temperature, unbound dyes were removed by gel filtration (Sephadex G-25). The molar ratio of myosin rods to bound dyes was approximately 1:1, assuming molar extinction coefficients for FITC at 495 nm of $7.6 \times 10^4\ M^{-1}\ cm^{-1}$ and for TRITC at 554 nm of $7.8 \times 10^4\ M^{-1}\ cm^{-1}$. Myosin was labeled with iodoacetamide rhodamine (IAR; Molecular Probes) by the same way as the labeling of myosin rods. The molar ratio of myosin to bound dyes was approximately 1:1, assuming molar extinction coefficients for IAR at 540 nm of $7.6 \times 10^4\ M^{-1}\ cm^{-1}$. IAR is expected to bind predominantly to a reactive cysteine (SH-1) in the myosin head.

Synthesis of fluorescently labeled myosin rod cofilaments

Myosin, myosin rod, and fluorescently labeled myosin rods were mixed in 0.6 M KCl, 5 mM $MgCl_2$, 10 mM HEPES, pH 7.0, and the mixture was dialyzed against a solution of 0.12 M KCl, 5 mM $MgCl_2$, 10 mM HEPES, pH 7.0, overnight at 0°C without stirring. Total concentration of proteins was set to 0.15 μM and the molar ratio of myosin to myosin rod in the mixtures was adjusted from 1:32 to 2:1. By this method, 5- to 8-μm-long filaments were obtained. It was confirmed by sodium dodecyl sulfate polyacrylamide gel electrophoresis that the composition in the cofilaments, after removal of nonpolymerized proteins, was the same as that in the original mixture of myosin and myosin rods (data not shown). Furthermore, to confirm the random co-polymerization of myosin and myosin rods, cofilaments were made from myosin with heads labeled with IAR and myosin rods labeled with FITC, and the fluorescence intensity from IAR-myosin and FITC-rods in each cofilament was measured. We found that the ratios of fluorescence intensities from IAR-myosin to that from FITC-rods in each cofilament was almost the same as others, indicating that the cofilaments have the same composition. The random distribution of myosin heads on the cofilaments was confirmed by immunoelectron microscopy (see Results).

The number of myosins per unit length of cofilament was determined from the fluorescence intensity of IAR-myosin in the cofilaments by comparing with the intensity of single actin filaments fully labeled with PHD-TRITC. As the number of actin monomers is approximately 360 per μm (Hanson and Lowy, 1963), the number of bound dye (tetramethylrhodamine) molecules per micron of filament should be 360 at full labeling.

The fluorescence intensity of the solution of actin filaments labeled with PHD-TRITC was 90% of that of myosin filaments labeled with IAR, in which the concentration of bound dyes was the same.

Electron microscopy

Synthetic myosin and myosin rod cofilaments were negatively stained with 1% uranyl acetate and observed by electron microscopy (JEOL-1200EX II). For immunoelectron microscopy, myosin filaments were mounted on a grid mesh covered with a carbon-coated formvar film. The mesh was blocked with a solution A (0.12 M KCl, 10 mM HEPES, pH 7.0, 5 mM $MgCl_2$) containing 5 mg ml^{-1} of bovine serum albumin (BSA) for 30 min. The samples were then exposed to 300X diluted polyclonal guinea pig antibody against rabbit myosin heavy chain for 2.5 h. After being washed with the solution A containing BSA, they were reacted with 5X diluted 5-nm gold conjugated goat anti-guinea-pig IgG (Zymed Laboratories, San Francisco, CA) for 2.5 h. After another washing with solution A, they were negatively stained with 1% uranyl acetate and observed by electron microscopy.

Observations of fluorescently labeled filaments and image processing

Single actin filaments and myosin rod cofilaments were observed with an inverted microscope (Olympus, IMT-2) equipped with epifluorescence optics, a Zeiss Neofluor 100× objective (oil immersion; NA 1.3) and a 100-W mercury arc lamp. Fluorescence images were videotaped with a high sensitivity television camera (Hamamatsu-Photonics, C-2741) and a video recorder. The fluorescence intensity, filament length, and sliding velocity of actin filaments and myosin rod cofilaments were measured by a computer image processor (Avio/Excel, Nippon Avionics Co., and Pc-9801 DA, NEC Co., Japan).

In vitro motility assay

For the filament assay, a solution containing myosin rod cofilaments was applied to a coverslip, pretreated with silicone (Harada et al., 1990) and albumin. Precoating with albumin (0.5 mg ml^{-1} BSA) was essential to obtain fast motion of actin. After 1 minute, unbound filaments were washed out with the assay medium (see below). Actin filaments, labeled with PHD-TRITC, were then added and the movement of the filaments observed by fluorescence microscopy (Harada et al., 1990). Single intact thick filaments of clam adductor muscle ~100 nm wide and 50–100 μm long were visualized under a fluorescence microscope as follows. The thick filaments were first bound to the surface of a coverslip and then TRITC-labeled albumin was applied. As fluorescently labeled albumin was bound to the coverslip surface but not to the thick filament, the filaments could be observed as dark lines under a fluorescence microscope.

For the surface assay, a myosin-coated surface was prepared by applying myosin dissolved in a high salt solution to silicone-pretreated surface of coverslips as described previously (Harada et al., 1990). HMM-coated nitrocellulose films were prepared by the method of Toyoshima et al. (1987).

All experiments were performed in an assay medium containing 25 mM KCl, 5 mM $MgCl_2$, 2 mM ATP, 20 mM HEPES, pH 7.6. To reduce photo-bleaching, 50 μg ml^{-1} glucose oxidase, 9 μg ml^{-1} catalase, 1.15 mg ml^{-1} glucose, and 0.5% 2-mercaptoethanol were added (Kishino and Yanagida, 1988; Harada et al., 1990).

ATPase activity and shortening velocity of single muscle fibers

The ATPase activity of single glycerinated rabbit psoas fibers was measured under isometric conditions by the method of Higuchi and Goldman (1991) with some modification. The fiber with full overlapping between thin and thick filaments (the sarcomere length, 2.2–2.3 μm) was immersed in a solution containing 90 mM KCl, 5 mM $MgCl_2$, 50 mM HEPES, pH 7.6, 0.1 mM $CaCl_2$, 50 μM diadenosine pentaphoshate (Sigma Chemical Co., St. Louis, MO), 0.5% 2-mercaptoethanol, 5 mM caged ATP, 2 mg ml^{-1} creatine kinase (250 U mg^{-1}; Sigma type I), and 3–10 mM creatine phosphate. The concentration of KCl was chosen to be compatible with the conditions of the in vitro assay (see Results). The fiber was then transferred to a fused silica trough containing silicone oil (Sin'etsu KF-96–100CS). The temperature of the trough was 27°C. The caged ATP photolysis was triggered by a UV pulse (300 μs in duration, wave length of 310–370 nm) from a Xenon flash lamp (Horiuti et al., 1993). The amount of caged ATP photolyzed into ATP was determined as follows. A small well (3 mm in diameter and 1 mm in depth) containing 0.5 mM caged ATP, 20 mM HEPES (pH 7.6), 0.6 M KCl, 10 mM EDTA, and 0.1 mg ml^{-1} myosin was illuminated by a UV pulse. The amount of released ATP was determined by measuring the amount of phosphate after hydrolysis by myosin for 10 min at 27°C. The amount of caged ATP photolyzed into ATP by a single flash was 29%.

The ATPase activity was determined by measuring the time until the muscle fibers went into rigor after activating them by photolysis of caged ATP in the presence of various concentrations of creatine phosphate. The state of the muscle fibers was monitored by measuring the stiffness (Horiuti et al., 1993). The stiffness was obtained from the tension response when sinusoidal length changes with amplitude of 0.1–0.3% of the fiber length were applied to the fiber. The frequency of applied length change was chosen to be 10 Hz because the difference between the fiber stiffness at contraction and rigor is large at low frequencies (Kawai and Brant, 1980).

The shortening velocity of muscle fibers, which was activated by photolysis of caged ATP, was measured by a slack method (Edman, 1979).

Preparation of the microneedles

Glass microneedles, approximately 0.3 μm in diameter were made from 1.1-mm-diameter glass rods using a glass electrode puller (Narishige PD-5). A microneedle was attached to a rigid glass rod (tip diameter ~5 μm) with epoxy resin and cut by a heated 5-μm-diameter platinum wire under a binocular microscope (Olympus SZH-10). The lengths of the microneedles were 50–100 μm. To increase contrast, a nickel particle, 1–2 μm in diameter, was attached to the tip with epoxy resin (Fig. 1 *a*; Ishijima et al., 1991). The stiffness of the microneedle (K_N) was determined by cross-calibration (see below) against a standard needle of known stiffness by essentially the same method described previously (Kishino and Yanagida, 1988). The stiffness of the standard needle was determined by measuring vertical bending due to the weight of the 25-μm-diameter steel wires. The weight of the wires (3.86 ± 0.07 mg m^{-1}; mean ± SD, n = 12) was determined by measuring its length under a microscope. The lengths of the wires used were 300–600 μm (1.2–2.4 μg in weight). The bending (4–58 μm) of a needle was measured for three different lengths of the wires and the measurements were repeated four times for each wire. The standard error was within 5%. Thus the stiffness of the standard needles (K_s, 0.4–2.5 pN nm^{-1}) was determined. The standard needle and the needle used for experiments were mounted on fine micromanipulators (Narishige WR-88). The tips of both needles were attached to each other, and the needle for the experiments was bent by moving the base of the standard needle in the range of 1–10 μm (p) under a microscope (Olympus, IMT-2). This cross-calibration was repeated 10–15 times and the stiffness of the needle (K_N) was determined from the average bending of the needle (q) as $K_N = \{q/(p - q)\}K_s$. The standard error was within 5% of the mean. The stiffness of needles used (K_N) was 0.03–9 pN nm^{-1}. The microneedle was coated with N-ethyl-maleimide (NEM)-treated myosin monomers to increase the affinity for an actin filament as described previously (Kishino and Yanagida, 1988).

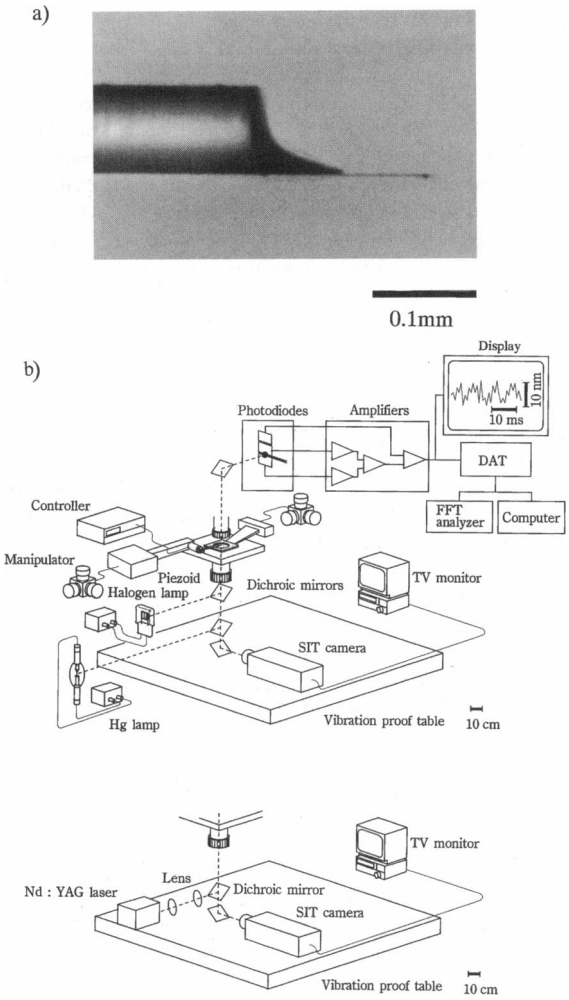

FIGURE 1 (*a*) Image of a glass microneedle taken by a dark-field microscope. (*b*) Schematic diagram of the high resolution force and displacement measurement system (see Materials and Methods for details).

Apparatus for nanometer-piconewton manipulation and data analysis

Fig. 1 *b* shows a schematic diagram of the apparatus for manipulating a single actin filament with a microneedle and measuring displacement of the microneedle. The set-up was built on an inverted fluorescence microscope (Olympus, IMT-2), modified to minimize mechanical vibrations and drift, and set on a vibration-free table (HELTZ, HG-107LM). Fluorescence of the labeled actin filament was excited by ~540 nm light from an ultra-high-pressure mercury lamp and a 100× oil immersion objective lens (ZEISS Neofluor, NA 1.3). The fluorescent image of the filament was displayed on a TV monitor by a high sensitivity SIT camera (Hamamatsu-Photonics, C-2741). The microneedle used to catch the actin filament was manipulated by a fine micromanipulator (Narishige, WR-88) and a piezo-actuator (Micro Kinetics Corp., CTC-6094–5, Tokyo, Japan). The displacement of the needle was measured as follows. The nickel particle attached to the tip of the needle was illuminated with 700- to 900-nm light from a highly stabilized halogen lamp (Phillips, model 13512, 12V, 50W) with 0.02% root mean square (rms) ripple of light intensity. Alternatively, a frequency-doubled Nd:YAG laser (Light Wave Electronics, model 140-0532-100, wave length = 532 nm, mode = TEM_{00}, maximal power = 100 mW, rms ripple = 0.02%) was used for both exciting the fluorescence of the actin and illuminating the nickel particle. When a coherent and monochromatic laser was directly introduced into a dichroic mirror, the light intensity was inhomogeneous because of interference at the specimen and the photodiodes. To minimize the inhomogeneity of the illumination by defocusing the interference patterns, a concave lens (f = 10 mm) and a convex lens (f = 70 mm) were placed 50 mm apart between the laser and the dichroic mirror (Olympus DM 580) (Fig. 1 *b*). Thus, the illumination could be homogeneous enough to observe the actin filament and measure the displacement of the microneedle.

The image of the nickel particle was projected onto a pair of photodiodes (Hamamatsu-Photonics, S2545) through an objective piece (Olympus, ULWD CDPlan ×40) with a long working distance of 5 mm and an eye lens (Olympus, ×10). The image of the nickel particle was magnified by 250× at the photodiodes. The photodiode outputs, converted into voltage by I-V converters (Analog Devices, AD-11, Japan), were subtracted, referred to the incident light intensity by a divider circuit (Analog Devices, AD-515), and recorded on tape by a digital data recorder (TEAC, RD-101T, Japan) at a sampling rate of 24 kHz. The response time to a sudden step light change, applied to the photodiodes by a light-emitting diode, was 16 μs (bandwidth, 10 kHz), limited by the feedback registers used in the I-V converters and stray capacitances. The differential output signals were analyzed off-line by a fast Fourier transform (FFT) analyzer (Advantest, R9211A) and a computer (NEC, PC-9801).

The displacement of the needle in the nanometer range was calibrated as follows. The differential output signals were measured when the photodiode pair, on which the image of the needle fixed on the stage was projected, was moved from 0.025 to 15 μm with the needle fixed. The photodiode pair was moved by a piezo actuator in the range of <1 μm and by a micromanipulator in the range of >1 μm. Displacements of 0.025–15 μm at the photodiodes correspond to those of the needle of 0.1–600 nm. Thus, the needle displacements were calibrated by using the relationship between the differential output signals and the displacements of the photodiode pair. As the relationship between the differential output and the displacement of needle was dependent on the size of nickel particles, the calibration was performed for each needle.

RESULTS

Performance of the apparatus

Fig. 2 shows the traces of differential output signals when a frequency-doubled YAG laser (Fig. 2, *a* and *b*) and a halogen lamp (Fig. 2, *c* and *d*) were used for illumination (the bandwidth, 10 kHz). Fig. 2, *a* and *c*, shows instrumental noise when light was on and Fig. 2, *b* and *d*, shows instrumental noise when light was off and a stiff (>100 nN nm^{-1}) needle, of which thermal vibration was negligible, was set. The instrumental noise when a laser was used was more than 10-fold smaller than that when a halogen lamp was used. However, the output signal when the laser was used for illumination was often unstable in the low frequency range of <1 Hz. Therefore, the laser was not suitable for recording slow events, whereas the signals obtained by the halogen illumination were noisier but more stable at low frequencies.

Fig. 2, *e* and *f*, shows the differential output signals when sinusoidal displacements with amplitudes of 0.1 and 1 nm were applied to the stiff needle, respectively. The output signals were recorded using the laser with a bandwidth of 10 kHz. The traces shown are single runs without averaging. Thus, the displacement of 0.1 nm could be clearly observed without averaging. The thermal vibrations of the needle were small because of its very high stiffness (>100 nN nm^{-1}). Fig. 2 *g* shows the

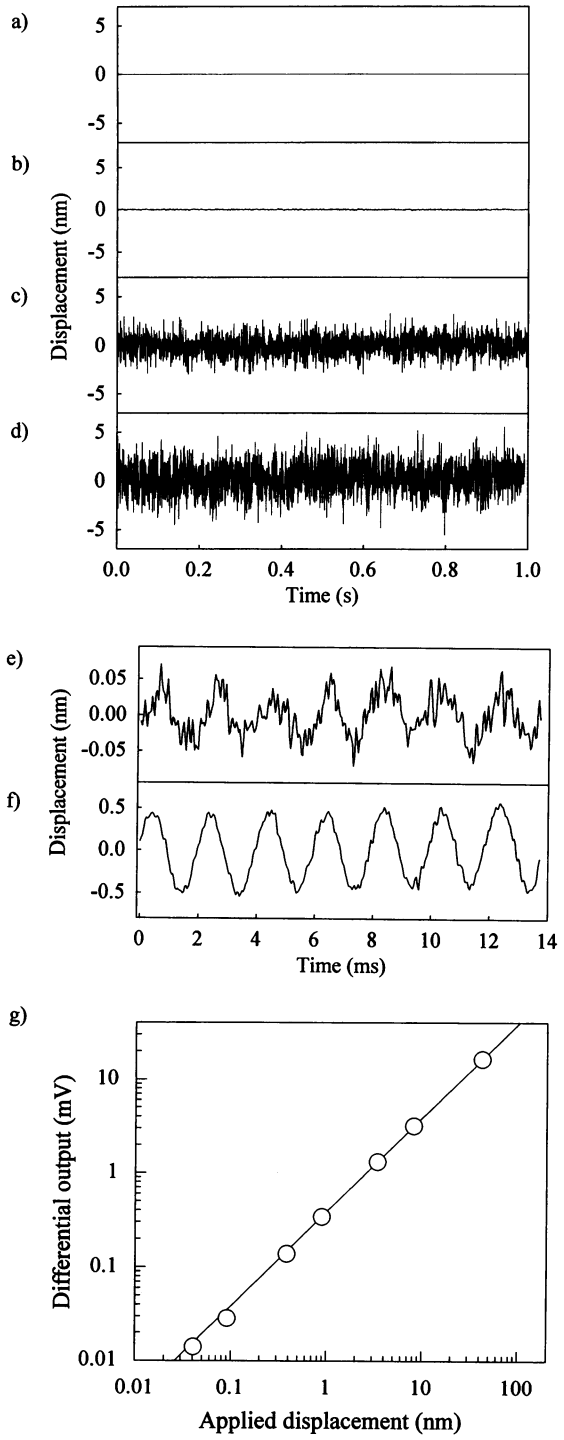

FIGURE 2 (*a–d*) Instrumental noise of the measurement system with a stiff (>100 nN nm^{-1}) needle set when the light was off (*a* and *c*) and on (*b* and *d*), recorded by using a laser (*a* and *b*) and a halogen (*c* and *d*) lamp, respectively. (*e* and *f*) Changes in the differential outputs from a pair of photodiodes when sinusoidal length changes were applied to the microneedle with amplitudes of 0.1 nm (*e*) and 1 nm (*f*). The signals were recorded with a 10-kHz bandwidth. The traces show single runs without averaging the signals or passing them through a filter. A frequency-doubled green YAG laser was used for illuminating the microneedle. (*g*) Relationship between displacements of the microneedle and differential outputs. Changes in the differential output when sinusoidal displacements were applied to the needle with amplitudes of 0.06–100 nm and 20 Hz. The output amplitudes were obtained from the power spectra using the FFT analyzer.

relationship between the amplitudes of sinusoidal displacements of the needle applied by the piezo actuator and the differential outputs. The outputs were obtained from the power spectra using the FFT analyzer. The outputs were linearly proportional to the amplitudes of displacements in the wide range from 0.06 to >50 nm. The same relationship was obtained by using a halogen lamp.

Measurements of thermal vibrations of microneedles

Thermal vibrations of microneedles with various stiffness were measured (Fig. 3 *a*). The amplitudes increased as the stiffness of the microneedles decreased. The stiffness of the needles was determined by the cross-calibration method (see Materials and Methods). Their power density spectra (PDS) are shown in Fig. 3 *b*. When a halogen lamp was used, the instrumental noise was as large as thermal vibrations of a needle of approximately 1.5 pN nm^{-1} in stiffness (Figs. 2 *d* and 3 *b*). Therefore, a laser was used to measure thermal vibration of needles. The PDS ($\Phi(f)$) of thermal vibrations of the needles are given, by solving a Langevin equation, as $\Phi(f) = 4\beta k_B T ((K - 4\pi^2 m f^2)^2 + 4\pi^2\beta^2 f^2)^{-1}$, where β is the friction coefficient of a needle against solution, k_B is the Boltzmann constant, T is absolute temperature, K and m are stiffness and mass of a needle, respectively, and f is frequency (refer to Kittel, 1958). If inertia is negligible, the power density is expected to be constant at low frequencies and decrease with frequency square (f^2) at the high frequencies, i.e., the spectrum is Lorentzian ($\Phi(f) = 4\beta k_B T/K^2 (1 + (f/f_c)^2)^{-1}, f_c = K (2\pi\beta)^{-1}$). The PDS fitted the Lorentzian curve when the stiffness of the needles was <3 pN nm^{-1}. The slope of the spectra in the high frequency region deviated from f^2 and approached f^4 as the stiffness was increased to >3 pN nm^{-1}, because the power spread in the high frequency region and so the value of $4\pi^2 m f^2$ was not negligible.

Mean square of the thermal vibrations of the needle ($\langle\Delta x^2\rangle$), obtained as $\int$ (PDS) df, should be combined with the stiffness of the needle by the equipartition law as $\frac{1}{2}K_N\langle\Delta x^2\rangle = \frac{1}{2}k_B T$ (refer to Kittel, 1958). The values of $k_B T (\langle\Delta x^2\rangle)^{-1}$ were plotted against K_N in Fig. 3 *c*. The relation was linear and the slope was approximately 1, in agreement with the equipartition law. Fig. 3 *d* shows the relationship between the stiffness of needles (K_N) and the corner frequency f_c, in which the power density is one-half of the maximal value (flat level). f_c gives the approximate measure of the response time of the needles. When the inertia of the microneedles is negligible, $(2\pi f_c)^{-1}$ gives the rise time (0–63%) of the displacement of the needles upon a sudden length change. f_c increased with increasing needle stiffness, K_N (Fig. 3 *d*). As f_c is a function of not only K_N but also the friction coefficient, β, i.e., $f_c = K_N (2\pi\beta)^{-1}$, f_c does not necessarily linearly

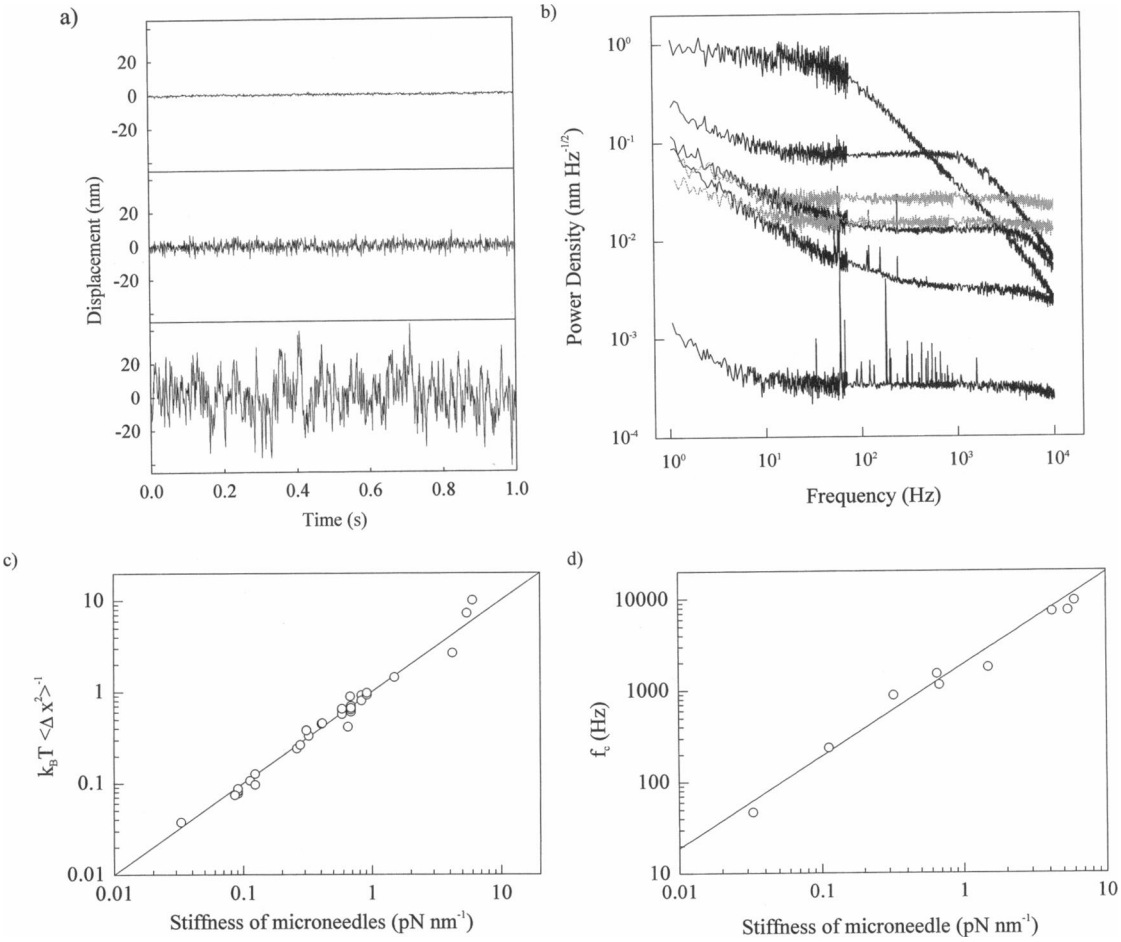

FIGURE 3 (*a*) Thermal vibrations of needles with various stiffness. The stiffness values of the needles were 4.2 (*upper*), 0.66 (*middle*), and 0.033 pN nm^{-1} (*bottom*), respectively. The bandwidth was 10 kHz. (*b*) The power density spectra (full-tone lines from bottom to top) of the differential output signals when light was off and on (instrumental noise) with a stiff (>100 nN nm^{-1}) needle set and thermal vibrations of the needles with stiffness of 4.2, 0.66, and 0.033 pN nm^{-1}. The signals were recorded by using a laser, except for the spectra, shown by gray lines, of the instrumental noise (*upper*, light on; *lower*, light off) recorded by using a halogen lamp. (*c*) Relationship of the stiffness of needles versus the root mean square of Brownian motions of the needles. (*d*) Relationship of the stiffness of needles versus the corner frequencies in the power density spectra of thermal vibrations of the needles. The length of needles used were approximately 100 μm, except for the most flexible needle (200 μm).

increase in proportion to K_N. As the most flexible needle (K_N = 0.03 pN nm^{-1}), which was difficult to make, was longer and thicker than stiffer needles, i.e., β was larger, f_c (40 Hz) was 2–3 times smaller than that (100 Hz) expected if the length were similar to that of stiffer needles (Fig. 3, *b* and *d*).

Orientation-dependent movements on a myosin rod cofilament

Electron micrograph of cofilaments and myosin head distribution

Long filaments, 5–8 μm in length, were synthesized by slowly copolymerizing a mixture of intact myosin and fluorescently labeled myosin rods (see Materials and Methods). The myosin filaments were bound to a siliconized coverslip. These copolymer filaments could be visualized by fluorescence microscopy without the myosin heads being labeled, which might alter their mechanochemistry. The density of myosin heads on the filament could also be varied by changing the molar ratio of myosin to rod. Fig. 4, *a–c*, shows the electron micrographs of the cofilaments with the myosin:rod ratios of 2:1, 1:9, and 1:32, respectively. The cofilaments with high ratios of myosin to rod (1:1) were cylindrical like intact thick filaments. In contrast, the sparse cofilaments with the low ratios of <1:2 appeared ribbon-like in electron micrographs, which was similar to that of paracrystals made from pure rods. They were ~0.2 μm wide at the center with tapered ends. To estimate the density of myosin heads in the filament, we made filaments from myosin with heads labeled with IAR- and FITC-labeled myosin rods. The ratios of fluorescence intensities from IAR-myosin and FITC-rods was approximately constant among the filaments, also indicating random copolymerization of myosin and myosin rods. The density of myosin on the surface of sparse filaments (myosin:rod, 1:9) was deter-

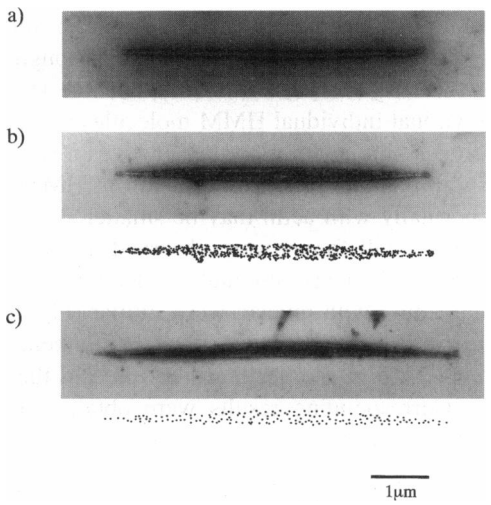

FIGURE 4 Negatively stained electron micrographs of synthetic myosin rod cofilaments with the myosin and rod molar ratios of 1:1 (*a*), 1:9 (*b*), and 1:32 (*c*). To see the position of the myosin heads, the filaments were labeled with primary antibodies against the myosin heads and secondary antibodies attached to 5-nm (average diameter) colloidal gold particles. The gold particles were not seen clearly at the magnification required to observe the whole filament, so the positions of the gold particles were observed at a high magnitude and plotted below the micrographs.

mined from the fluorescence intensity of IAR-myosin in the filaments on the basis of the intensity of single actin filaments fully labeled with PHD-TRITC. The density was 375 ± 40 myosin molecules per μm (mean ± SE, $n = 14$). Next, to examine whether the distribution of myosin heads is random, the cofilaments were labeled with primary antibodies against the myosin heads and secondary antibodies attached to 5-nm colloidal gold particles. The immunogold particles bound to myosin heads were not seen clearly at the magnification required to observe the whole filaments, so the position of the gold particles observed at a higher magnification were plotted below the images. The average density of the particles was 800 μm^{-2}. As the density estimated from the fluorescence intensity is 375 two-headed myosin molecules μm^{-2}, the average number of gold particles per head is approximately 1. When the content of myosin was further (less than threefold) reduced, i.e., the molar ratio of myosin to rod was 1:32, the density of gold particles was, in parallel, reduced to ~250 μm^{-2}. The autocorrelation function of the positions of the gold particles showed that the distribution of particles is almost random, except for a small peak corresponding to the two-headed structure of the myosin molecule in the perpendicular direction (~15 nm). The bare zone, seen in the center of pure myosin filament and high ratio cofilaments, was not clear. However, both sliding velocity and force depended on the polarity of cofilaments (Table 1), similar to those on the high ratio cofilaments. This result indicates that myosin molecules are oriented in a bipolar fashion as they are in the high myosin-to-rod ratio cofilaments.

TABLE 1 Forces and velocities on single myosin filaments and in random *in vitro* assays

	Force (pN (μm actin filament)$^{-1}$)	Velocity (μm s^{-1})
Synthetic myosin filament		
Forward direction		
1:9*	32 ± 5 (19)	9.3 ± 0.4 (76)
1:1	36 ± 7 (13)	10 ± 0.2 (79)
2:1	52 ± 5 (53)	9.8 ± 0.2 (162)
Backward direction		
1:9	<3	2.6 ± 0.1 (57)
1:1	—	—
2:1	4.4 ± 0.7 (12)	2.5 ± 0.1 (133)
Intact clam filament		
Forward direction	36 ± 6 (8)	12.5 ± 0.2 (103)
Backward direction	2.8 ± 0.9 (16)	3.6 ± 0.1 (88)
Surface assays		
Myosin bound to silicone-treated coverslip	29 ± 3 (20)	8.6 ± 0.5 (30)
HMM bound to a nitrocellulose film‡	3.4 ± 0.4 (15)	7.2 ± 0.4 (50)

Data are given as mean ± SE for the number of experiments or actin filaments indicated in the parentheses. All experiments were performed at 27°C, expect for that shown in the bottom row, which was performed at 30°C.

*Myosin-to-rod ratio.

‡The HMM-coated surface was made according to the method of Toyoshima et al. (1987). Densities of myosin and HMM, determined by measuring EDTA-K^+ ATPase rates (Toyoshima et al., 1990; Harada et al., 1990), were both 2500 ± 500 μm^{-2}.

Movements of actin filaments

Fig. 5 shows fluorescence images of a myosin rod cofilament labeled with FITC (upper panel) and sequential fluorescent images of an actin filament labeled with PHD-TRITC, sliding along the cofilament in the normal physiological direction (toward the center of the filament, lower left) and in the opposite direction (away from the center, lower right). The average velocity in the forward direction was ~10 μm s^{-1} at 27°C, independent of the density of myosin (Table 1). This velocity was very close to the filament sliding velocity found in muscle fibers under comparable conditions (Fig. 8 *a*). The forward velocity was approximately fourfold larger than the backward one (Table 1). Similar results were obtained using intact thick filaments of clam adductor muscle (Table 1).

The velocity of actin filaments in the surface assay, in which myosin molecules were randomly coated on a silicone-treated surface, was similar to that in the forward direction (Table 1). The result agrees with the previous results that the velocity is dominantly determined by the myosin molecules that are correctly oriented relative to the actin filament (Yamada et al., 1990; Sellers et al., 1991; Saitoh et al., 1994).

Orientation-dependent force on a cofilament

Forces generated by the interacting actomyosin complexes were measured by catching one end of an actin filament on a

fine glass needle and then bringing the other end into contact with an immobilized myosin rod cofilament in the forward and the backward directions. The forces were measured from the displacement of the needle using the high resolution measurement system (Fig. 1 *b*). Fig. 6 *a* shows the fluorescent images of single myosin filaments before interaction with actin (upper panels in Fig. 6 *a*) and during force generation (lower panels in Fig. 6 *a*) and the time course of the force generation (needle displacement) in the forward (Fig. 6 *b*) and backward (Fig. 6 *c*) directions. The arrows indicate the times when actin interacted with the myosin rod cofilament. In the forward direction, a large force developed to reach a plateau with strong fluctuations. To approach the isometric condition, we used stiff needles resulting in an average needle displacement of only 6 nm. The average forces per unit length of actin filament interacting with myosin rod cofilaments in the forward direction were 32, 36, and 52 pN μm^{-1} at myosin:rod ratios of 1:9, 1:2, and 2:1, respectively (Table 1). The force did not decrease in proportion to the myosin content at low ratios. This is probably because the backbone of cofilaments with high myosin-to-rod ratios is very thin (~20 nm in diameter), so that a large number of heads would be easily bound to the surface to lose the ability to interact with actin, whereas that of cofilaments with low ratios is wide (~200 nm) and ribbon-like (Fig. 4), so that most of the myosin heads on the wide backbone would be active without binding to the surface.

The forces in the surface assays are also shown in Table 1. In the myosin-coated surface, the force was as large as in the myosin filaments. But, as the surface was fully coated with myosin molecules, the average force per head would be considerably smaller, as shown below. The force in a HMM-coated surface was much smaller, although the surface was similarly saturated with HMM (Table 1). As it has been shown that individual HMM molecules on the surface can produce a similar force to that of myosin (Finer et al., 1994; Ishijima et al., 1994), the fraction of HMM that can interact normally with actin may be smaller.

Only very small forces were observed in the backward direction on cofilaments, although the lengths of actin filaments interacting with myosin were similar (Fig. 6 *c*). The backward force per unit length of actin filament was approximately 10-fold smaller than the force in the forward direction. Corresponding results were obtained for intact thick filaments of clam adductor muscle (Fig. 6, *d* and *e*, Table 1).

Thus, the force and velocity are both strongly dependent on the relative orientation of actin and myosin.

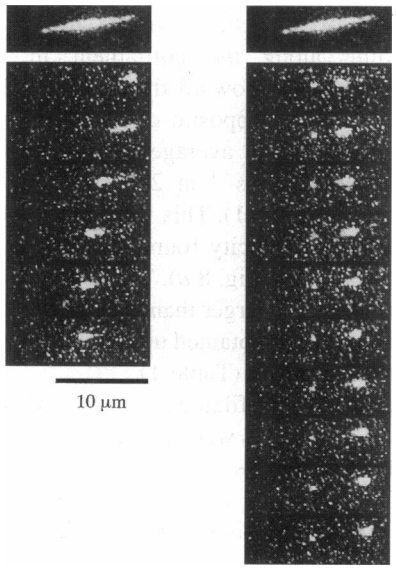

FIGURE 5 The upper panels show the fluorescence images of a myosin rod cofilament in which the molar ratio of myosin to myosinrods is 1:9. Myosin rods were labeled with FITC. The lower panels show sequential images, taken at 0.1-s intervals, of a fluorescent actin filament sliding in the forward (left) and backward (right) directions. The pictures are from a sequence in which the same actin filament traveled forward, turned, and then traveled backward on the same myosin filament. The actin filament was labeled with phalloidin-TRITC.

Orientation-dependent stiffness on a cofilament

Fig. 7 shows the stiffness of actin-myosin interaction during force generation in the forward direction when the stiff (1 pN nm^{-1}) needles were used. A 2-nm sinusoidal displacement with the frequency of 100 Hz was applied to the base of the needle. The stiffness was obtained by measuring the amplitude of the sinusoidal displacement at the tip of the needle with the FFT analyzer as previously described (Ishijima et al., 1991). The stiffness in the forward direction was 0.024 ± 0.0019 pN nm^{-1}/pN force (n = 13). This value is 2-fold larger than that previously measured in a randomly oriented myosin-coated surface (Ishijima et al., 1991). When the actin filament was interacted in the backward direction with a cofilament, the stiffness was too small to detect (at least 10-fold smaller than that in the forward direction). The results indicate that the stiffness of actin-myosin interaction in the backward direction is also much smaller than that in the forward direction.

ATPase activity and shortening velocity of single muscle fibers

The ATPase activity has been directly measured in the previous surface assays (Toyoshima et al., 1990; Harada et al., 1990; Uyeda et al., 1990), but these assays neglect the effect of random orientation of myosin molecules. In the present filament assay, we could not measure ATPase activity directly because cofilaments were not homogeneously bound to the surface at a high density without filament overlap, and actin filaments moved both in the forward and backward directions. Therefore, the ATPase activity was measured using glycerinated rabbit psoas fibers under conditions comparable to those in the filament assay. As the sliding velocity and force in the filament assay were both similar to those in muscle (see Discussion), the elementary process of sliding force generation in the present in vitro assay would be close to that in contracting muscle. However, the affinity of myosin heads for actin in the

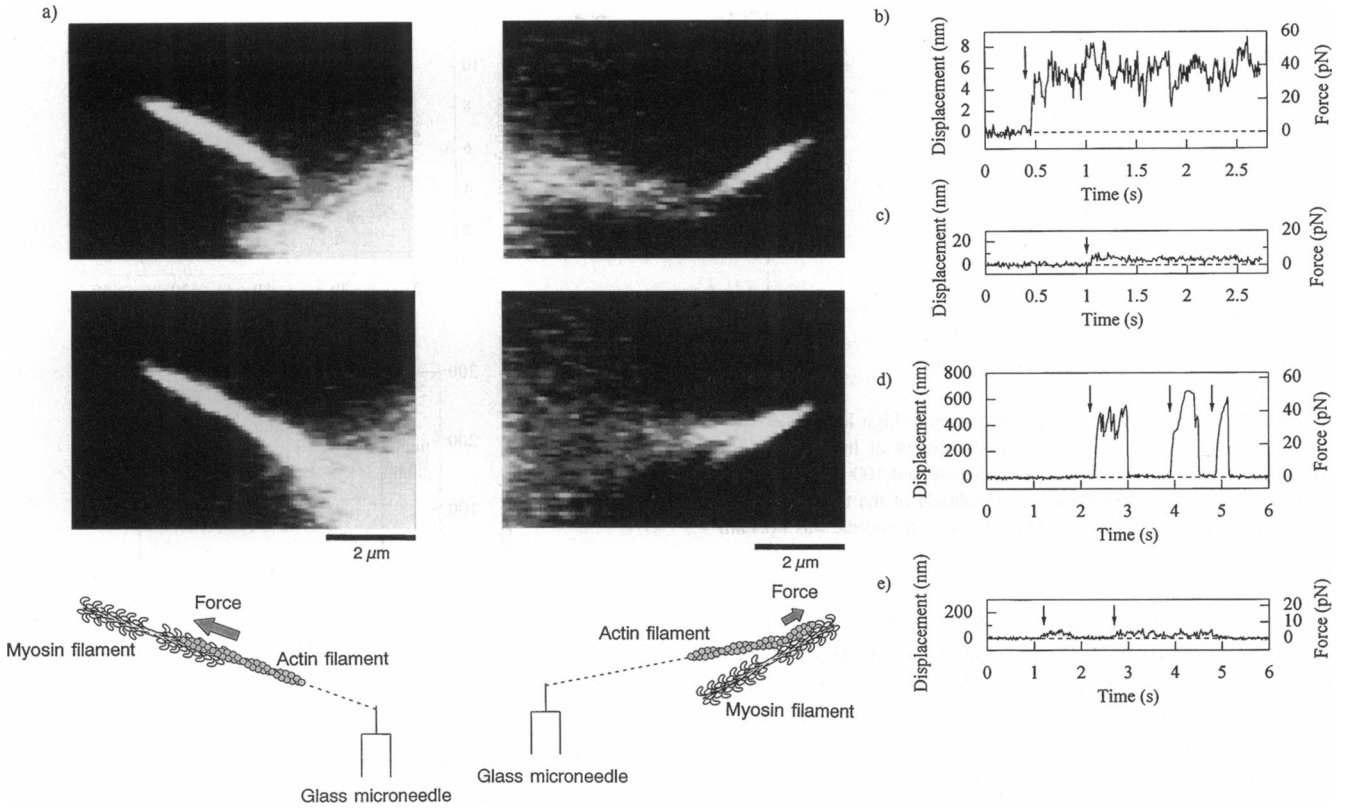

FIGURE 6 Force measurements in the forward and backward directions on single myosin filaments. (*a*) Top panels show the fluorescence images of single myosin rod cofilaments on coverslips. Myosin:rod molar ratio was 2:1. To see the actin and myosin filaments at the same time, myosin rods were labeled with the same dye, TRITC, as the actin filaments. To clearly demonstrate the fluorescence image, a filament with a high content of fluorescently labeled myosin rods (16%) is shown. To make the image of actin filaments more distinct, myosin filaments with a lower content of fluorescently labeled rods (8%) were usually used. Middle panels show the fluorescence images of thick filaments interacting with phalloidin-TRITC-labeled actin filaments generating force in the forward (left) and backward (right) directions. Bottom panels show a schematic diagram of the force measurements. As the angle (θ) between the actin and myosin filaments was not zero, the force was corrected as the observed force $\times$ ($\cos^{-1}\theta$). When the actin filament was not perpendicular to the needle, the force was similarly corrected. (*b* and *c*) The time courses of force development in the forward and backward directions, respectively. Bandwidth, 50 Hz. The stiffness values for the needles were 6 pN nm^{-1} (*b*) and 0.7 pN nm^{-1} (*c*), respectively. Arrows indicate the times when the actin filaments interact with the cofilaments. (*d* and *e*) The time courses of force development in the forward (*d*) and backward (*e*) directions, respectively, on an intact clam thick filament. Bandwidth, 50 Hz. The stiffness value for the needle was 0.08 pN nm^{-1}. Therefore, the force fluctuations were attenuated (Ishijima et al., 1991). Arrows indicate the times when the actin filaments interact with the thick filaments.

present in vitro system is probably lower than that in a muscle fiber under identical medium conditions, because the density of actin and myosin filaments is much higher in the fiber. Therefore, the difference was adjusted by altering the concentration of KCl as follows. The velocity in vitro was almost constant in the range of 40–80 mM KCl and declined at lower concentrations. The velocity at 25 mM KCl was approximately 90% of maximum. A similar tendency was observed in muscle fibers, but the concentration of KCl that gave the 90% velocity relative to maximal (10.5 $\pm$ 0.6 μm s^{-1}) was approximately 90 mM (Fig. 8 *a*). Therefore, assuming that 25 mM KCl in vitro corresponds to 90 mM KCl in muscle, we measured the ATPase activity at 90 mM KCl and 27°C under otherwise identical conditions.

The ATPase activity of a muscle fiber was measured using caged ATP (see Materials and Methods). It was difficult to measure the ATPase activity of skinned muscle fibers activated by exchanging the bathing solution with that containing ATP at 27°C, because the force increased to reach its peak but then rapidly dropped and the sarcomere structure was irreversibly disordered during contraction at such a high temperature. This problem has been overcome using caged ATP. The muscle fiber activated by photolysis of caged ATP generated constant force and its sarcomere structure was kept orderly for a sufficiently long time to measure the ATPase activity (Higuchi and Goldman, 1991). This is probably because the muscle fiber was uniformly activated at once by caged ATP. The isometric force was 261 $\pm$ 35 kN m^{-2} or 1.6 $\pm$ 0.2 pN/head assuming the concentration of myosin heads in rabbit psoas fiber to be 0.24 mM (Tregear and Squire, 1973), which was similar to that when activated by ATP. The ATPase activity was obtained by measuring the time until the muscle fiber went into rigor after photolysis of caged ATP at various concentrations of creatine phosphate. The state of muscle fibers was monitored by measuring the stiffness (see Materials and Methods). The relative stiffness, normalized by the rigor

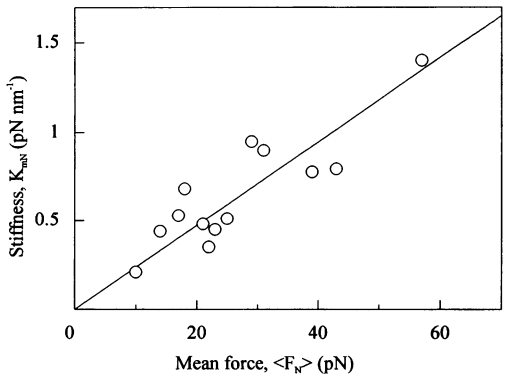

FIGURE 7 Stiffness during force generation at high load. The stiffness was determined by monitoring the tip movement of the needle when a sinusoidal length change with a 2-nm amplitude and 100-Hz frequency was applied to the base of the needle. The amplitude of the tip movement was measured by using a FFT analyzer. The stiffness of the needle was 1 pN nm^{-1}.

stiffness, was first constant for some period and then gradually increased to 1 (Fig. 8, *b* and *c*). This is because the muscle fibers were in the contracting state at the saturated ATP concentrations and then went into rigor gradually as the concentration of ATP decreased. The times at relative stiffness of 0.6, 0.7, 0.8, and 0.9 were measured at 3, 6, and 10 mM creatine phosphate. The differences between the times at 3 mM and at 6 and 10 mM creatine phosphate were measured at each relative stiffness and all averaged. Fig. 8 *d* shows the averaged differences. The ATPase activity was obtained from the slope of Fig. 8 *d* as $V_{ATP} = (\text{slope})^{-1} \times$ (concentration of myosin head in the fiber)$^{-1} \times$ (fractional space available for creatine phosphate). The slope was 0.45 ± 0.03 s mM^{-1} (n = 20). The fractional space available for creatine phosphate was calculated to be 0.84, according to the method of Matsubara et al. (1984). In this calculation, we assumed the molecular size of creatine phosphate to be 0.4 nm in radius and the lengths of A and I bands of 1.6 and 0.65 μm, respectively, and for other parameters the same ones as used by Matsubara et al. (1984) were assumed. The V_{ATP}, thus obtained was 7.8 ± 0.4 s^{-1}/head (n = 20) at 27°C .

Force fluctuations by multiple myosin heads and noise analysis

Kinetic characteristics of individual myosin heads could be evaluated using the fluctuations of the needle displacement when force was produced in the forward direction at near isometric conditions (Fig. 6 *b*). The PDS (Fig. 9 *a*) of the force fluctuations were Lorentzian with a corner frequency of 5.4 ± 0.4 Hz (Table 2). The relationship between the rms of force fluctuations ($\sqrt{\langle \delta F_N^2 \rangle}$) and the square root of mean force ($\sqrt{\langle F_N \rangle}$) was linear with slope $\sqrt{\langle \delta F_N^2 \rangle}$ $(\sqrt{\langle F_N \rangle})^{-1}$ = 1.95 ± 0.11 $\sqrt{\text{pN}}$ (Fig. 9 *b*, Table 2). These results suggest that, near isometric conditions, the myosin heads fluctuate stochastically and independently between low force and high force states. This point was supported by

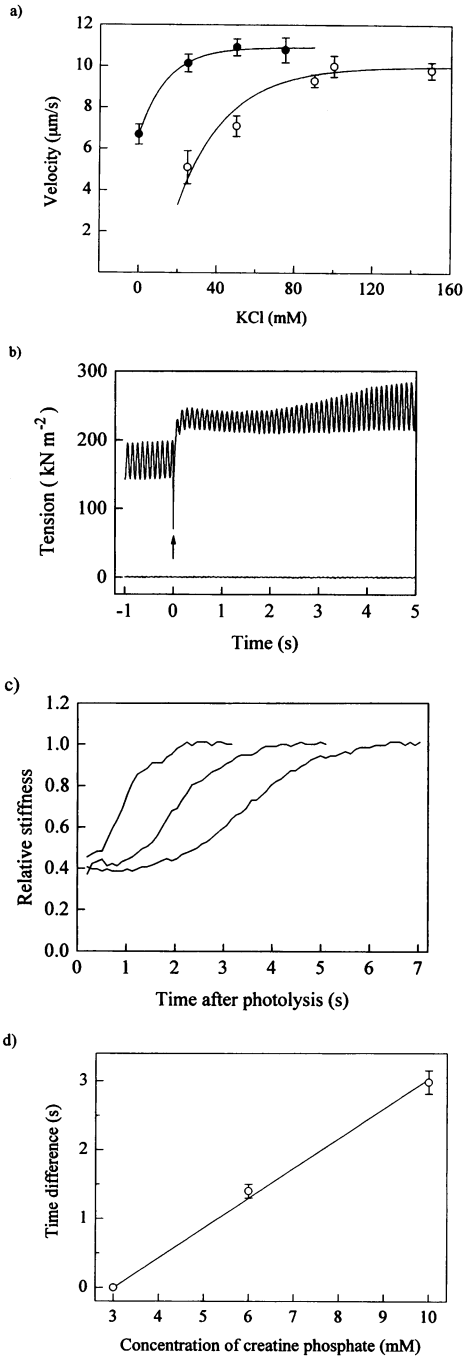

FIGURE 8 ATPase rate measurements of a skinned muscle fiber during isometric contraction. (*a*) Dependence of velocities of actin filaments along myosin filaments in the in vitro filament assay (●) and in muscle (○) on the KCl concentrations. Temperature, 27°C. See in vitro motility assay in Materials and Methods for other conditions. (*b*) Time course of force generation and change in the stiffness of a skinned muscle fiber when muscle contraction was triggered by photolysis of caged ATP. Arrow indicates the time when caged ATP was photolyzed by a xenon flash lamp. To monitor the stiffness, sinusoidal length change, with amplitude of 1 nm (half-sarcomere)$^{-1}$ and frequency of 10 Hz, was applied to the muscle fiber. The lower trace is for the relaxed state. Creatine phosphate, 10 mM; temperature, 27°C. (*c*) Time courses of changes in the stiffness of a muscle fiber after photolysis of caged ATP in the presence of creatine phosphate (from left to right) of 3, 6, and 10 mM. (*d*) The average differences of times when the relative stiffness of muscle fibers were 0.6–0.9 at 6 and 10 mM creatine phosphate from those at 3 mM creatine phosphate.

TABLE 2 Parameters estimated from noise analysis of force fluctuations based on the random on-off model

V_{ATP} (s^{-1})	7.8 ± 0.4 (20)*
f_c (Hz)	5.4 ± 0.4 (12)
$(\sqrt{\langle \delta F_N^2 \rangle}/\sqrt{\langle F_N \rangle})(\sqrt{pN})$	1.95 ± 0.11 (28)
k_+ (s^{-1})	12 ± 2
k_- (s^{-1})	22 ± 4
p_0	0.36 ± 0.07
F_0 (pN)	5.9 ± 0.8
$\langle F \rangle$ (pN)	2.1 ± 0.4

Data are given as mean ± SE for the number of experiments indicated in the parentheses. Data obtained using filaments with myosin and rod at the molar ratios of 2:1, 1:1, and 1:9 were mixed, because they were independent of the ratio. Calculated values are shown as the mean ± possible error $(\{\sum [\sigma_i^2(\partial\mu'/\partial x_i)^2]\}^{1/2}$, σ_i, the variance of the individual data point x_i; μ', the mean, Bevington et al., 1969).

*The actin-activated ATPase activity of myosin heads during isometric contraction of single glycerinated rabbit psoas fibers.

the force measurements using very sparse cofilaments, as shown later. Therefore, the data were analyzed using a simple, random on-off kinetic model (see Appendix). In this analysis the myosin heads are assumed to occupy either the on state, in which the force is F_o, or the off state (force = 0). F_o is constant in any particular on state and may vary among the on states. When F_0 varies among the on states, the F_0 calculated from the analysis indicates the average force in the on states. The variance of F_0 would actually be small, considering the variance of peak values of force spikes recorded from single molecules is small ((variance)$^{1/2}$ = 0.9 pN. see Fig. 11 *b*). Transitions between states occur randomly and independently.

Using this model, the mean force of a myosin head ($\langle F \rangle$) can be obtained analytically from the corner frequency, f_c, the ratio, $\sqrt{\langle \delta F_N^2 \rangle}$ $(\sqrt{\langle F_N \rangle})^{-1}$, and the ATPase activity, V_{ATP} (see Appendix). The values of f_c and $\sqrt{\langle \delta F_N^2 \rangle}$ $(\sqrt{\langle F_N \rangle})^{-1}$ were obtained from the spectra of the fluctuations (Fig. 9 *a*) and the slope of Fig. 9 *b*, respectively. As mentioned above, we used the ATPase activity of muscle fibers during isometric contraction (7.8 ± 0.4 s^{-1}/head) as V_{ATP}.

Using these values, the mean force obtained for the on state was F_o = 5.9 ± 0.8 pN/head, and the force averaged over the whole ATPase cycle time was found to be $\langle F \rangle$ = 2.1 ± 0.4 pN/head. The on (k_+) and off (k_-) rate constants were also obtained from the same analysis; k_+ = 12 ± 2 and k_- = 22 ± 4 s^{-1}, leading to a duty ratio (k_+ (k_+ + k_-)$^{-1}$) of 0.36 ± 0.07 (Table 2). With this model adjusted to fit the experimental data, each on-off cycle could be related to one ATPase cycle at high load.

Another solution of the quadratic equation for k_+ and k_- is possible (see Appendix). This solution leads to F_o = 11 pN, but such large force spikes were not observed when the density of myosin in cofilaments was greatly decreased, as shown later. Therefore, this solution is unlikely.

In this analysis, we used the ATPase activity of isometrically contracting muscle. Although we measured that under comparable conditions, there is still no guarantee that

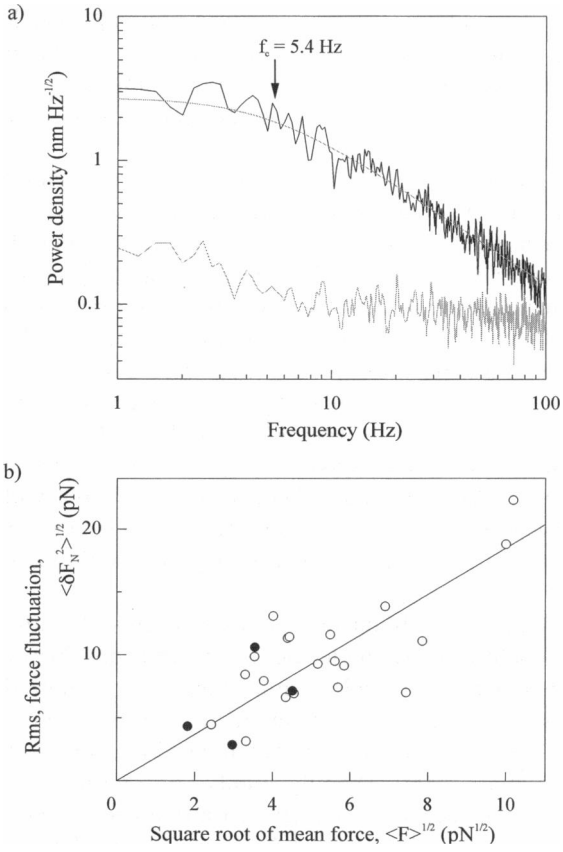

FIGURE 9 (*a*) PDS (*upper trace*) of the force fluctuations in the forward direction at high load recorded with a bandwidth of 10 kHz. The broken line shows a Lorentzian curve with corner frequency, f_c, of 5.4 Hz. The lower trace shows the PDS of the free needle with the stiffness of 6 pN nm^{-1}. A halogen lamp was used for illuminating the needle. (*b*) Relationship between square root of mean force and root mean square of force fluctuations. ●, myosin:rod ratio = 1:9; ○, myosin:rod ratio = 2:1.

the ATPase activity in the in vitro assay coincides with that in muscle. But, even if the ATPase activity varies in the wide range from 8.5 to 4 s^{-1}/head, F_0 changes from 7.6 to 4.4 pN and k_- changes from 17 to 29 s^{-1}, which are both not much different from those estimated above (5.9 pN and 22 s^{-1}, respectively). There is no solution at >8.5 s^{-1}/head.

Force and displacement from single myosin molecules

We tested whether the kinetic characteristics of individual heads estimated from the multi-molecule data can be directly observed in single-motor force recordings, analogous to the case of single and multiple ion channel currents recorded from biological membranes. To reduce the number of myosin heads that could interact with actin, we used myosin rod cofilaments with a myosin:rod ratio of 1:32, i.e., a myosin content of 3%. Such filaments appeared ribbon-like in electron micrographs (Fig. 4 *c*). They were ~6 μm in length and ~0.2 μm wide at the center with tapered ends similar to paracrystals made from pure rods. The density of myosin molecules on the surface of the filament, estimated

from the fluorescence intensity (see Materials and Methods), is approximately 100 μm^{-2} based on a random distribution as indicated by the positions of immunogold particles bound to myosin heads on the sparse myosin filament (Fig. 4 *c*, lower).

Force recordings were performed when one end of an actin filament was brought into contact with a myosin filament and became taut (Fig. 10 *a*). Occasionally, the tip of the actin filament slid over the center of the myosin filament and on to the other side (backward region), and a small length (<1 μm) of the actin filament interacted in the correct direction with the forward region of the cofilament. Thus, one end of the actin filament was caught by the needle and the other end was weakly held in the backward region. In this situation, large spike-like forces were generated (Fig. 10, *b–e*). When an actin filament interacted only with the backward region, the actin filament was just held there, and the sliding force was so small (<1 pN) it could hardly be detected.

With sparse cofilaments and short lengths of actin, only one or a few myosin molecules can reach actin. To estimate the number of molecules within range, we assume that a myosin molecule can reach an actin filament within a distance equal to the size of a myosin head (~30 nm) (Toyoshima et al., 1990). Then the number of myosin molecules that can interact with a 0.5-μm actin filament is 100 μm^{-2} × 30 nm × 0.5 μm = 1.5. A similar number can be obtained from force placed on an actin filament upon interaction with a myosin rod cofilament. The number of myosin molecules that can interact with a 0.5-μm actin filament is estimated as (force per 0.5-μm actin filament/force per myosin molecule) = 16 pN/(2.1 pN × 2) = 4 at the myosin:rod ratio of 1:9 (Tables 1 and 2). Therefore, the number of myosin molecules that can interact with a 0.5-μm actin filament would be 1.2 at the myosin:rod ratio of 1:32. Thus, individual mechanical events produced by single myosin molecules are expected to be observed with a myosin rod cofilament with the myosin:rod ratio of 1:32. When more sparse cofilaments with the molar ratio of <1:32 were used, the force spikes were hardly observed.

At high load

Fig. 10 *b* shows these spikes when a relatively stiff needle (1.6 pN nm^{-1}) was used so that the average needle displacement was as small (~4 nm) as in Fig. 6 *b*. We scored force spikes according to the following criteria. Fig. 11 *a* showed the PDS of signals without passing through a low-pass filter (detector bandwidth, 10 kHz). The power density of signals was in the frequency range from 1 to 50 Hz. Therefore, first we reduced electric and photon noise and noise due to thermal vibrations of a needle by passing the outputs through a low-pass filter with a bandwidth of 50 Hz (Fig. 10 *b*). We scored force spikes with durations larger than 15 ms (corresponding to the frequency of 10 Hz i.e., $(2\pi \times 15\ ms)^{-1}$). As the power integrated from 0 to 10 Hz is approximately 70% of total (Fig. 11 *a*), this procedure

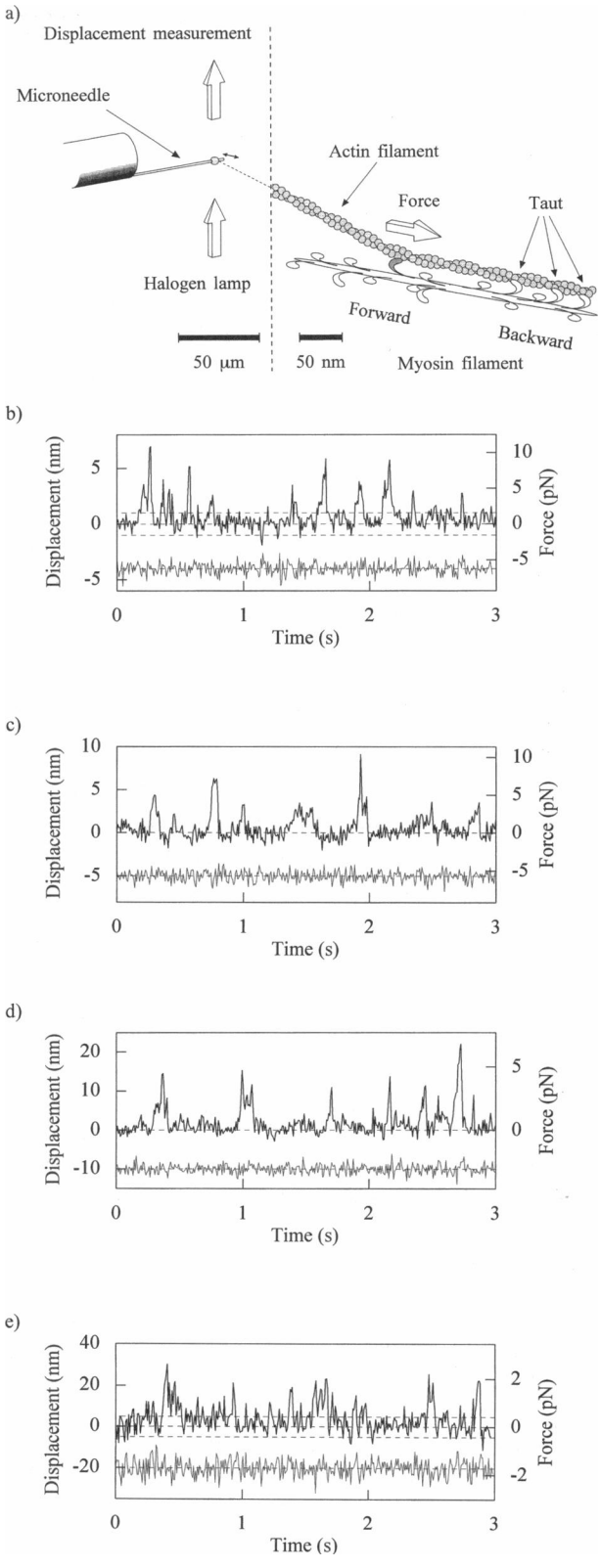

FIGURE 10 (*a*) Schematic diagram of the measurements of force and displacement spikes from single myosin molecules (see text). Force and displacement spikes at high load (*b* and *c*; needle stiffness K_N, 1.6 and 1.1 pN nm^{-1}, respectively), middle load (*d*; K_N, 0.31 pN nm^{-1}), and low load (*e*; K_N, 0.09 pN nm^{-1}). The lower traces indicate thermal vibrations of free needles. Broken lines in *b* and *e* show ±1 nm and ±5 nm, respectively. Temperature, 27°C for *b–d* and 21°C for *e*. Bandwidth, 50 Hz (see text).

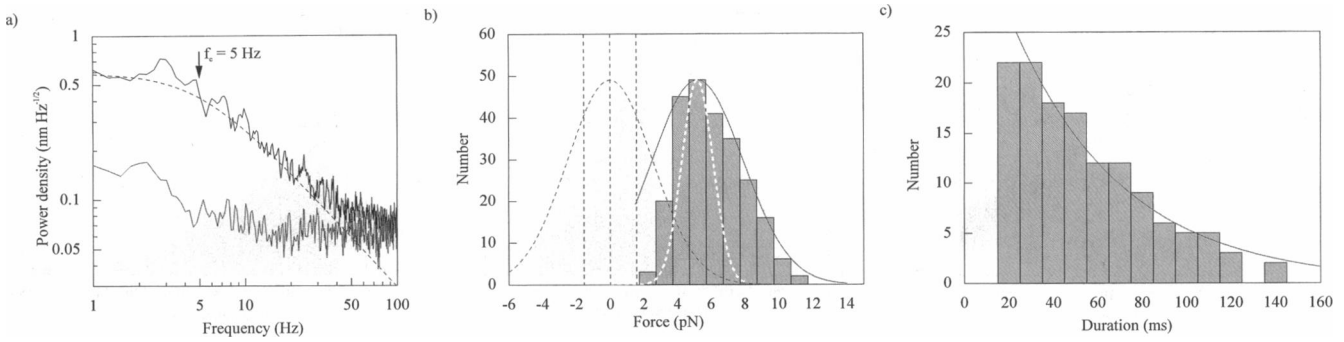

FIGURE 11 (*a*) PDS of force spikes shown in Fig. 10 *b*. The lower trace indicates that of thermal vibrations of a free needle (K_N = 1.6 pN nm^{-1}); 1 nm corresponds to 1.6 pN. (*b*) Histogram of the peak values of force spikes at high load. The force spikes were scored according to the criteria shown in text. Solid, broken, and dotted lines indicate the best fit Gaussian to the displacement histogram, the Gaussian distribution of the thermal vibrations when force spikes are not observed, and the subtracted Gaussian curve, respectively (see Discussion). Force spikes, of which heights were within 1.6 pN, were not scored (see text). (*c*) Histogram of the durations of the force spikes directly measured. A solid line indicates an exponential curve fitted over the histogram (τ = 50 ms).

would score approximately 70% of all force spikes. Force spikes smaller than 1.6 pN (corresponding to needle displacement of 1 nm) were omitted, as it was impossible to distinguish the force spikes from the thermal vibrations of a needle (Fig. 10 *b*, lower trace). Fig. 11 *b* shows the histogram of the peak values of force spikes scored as above. The histogram approximately fitted a single broad Gaussian distribution with the maximum near 6 pN and the width at the half-maximum of 6 pN (corresponding to needle displacement of 4 nm), but this broad distribution would be due mostly to the randomizing effect of the thermal vibration of the needle (see Discussion).

The corner frequency of the PDS was 5 Hz (Fig. 11 *a*). The sum of transition rates into (k_+) and out of (k_-) the force generation state is given by $2\pi \times 5$ Hz = 31 s^{-1}, based on the on-off random kinetics model (see Appendix). Fig. 11 *c* shows the histogram of the durations of the force spikes at half the maximum directly measured. The average duration, which was obtained by fitting a single exponential curve, $e^{-t/\tau}$, to the histogram, was approximately 50 ms, i.e., k_- = 20 s^{-1}. The number of force spikes per second was approximately 7, i.e., the average interval between adjacent force spikes was 140 ms, corresponding to k_+ = 11 s^{-1} ((140 − 50)$^{-1}$ ms^{-1}). Thus, $k_+ + k_-$ = 31 s^{-1} was in good agreement with the corner frequency of the PDS. This agreement indicates that most of the force spikes observed do not overlap with each other but are well separated, as the former value shows the duration of individual spikes, independent of whether the force spikes are overlapped.

Sparser force spikes (f_c = 3.4 Hz, k_+ = 1 s^{-1}) were sometimes observed in the cofilaments with the same myosin:rod ratio (1:32). The big variety of the transient rates into the force generation state (k^+) would be due to the difference of the geometric arrangement between the actin filament and the myosin molecule. If the actin filament is placed just near the myosin molecule, the transient rate k_+ would be large (Fig. 10 *b*). Whereas, if the actin filament is placed far from the myosin molecule, the probability that the myosin head encounters the actin filament would be small and consequently k_+ would be small (Fig. 10 *c*). Although k_+ or the frequency of spikes had a large variety, the peak force (F_o) and the duration of the spikes ($1/k_-$) were approximately constant, independent of the frequency of the spikes (Fig. 10 *b* and *c*). This also confirms that the observed force spikes are produced by single myosin molecules (or heads).

Thus, the mean peak value of force spikes and the transient rate out of the force generation state (k_-) are consistent with those deduced from the noise analysis of force fluctuations (Table 2).

At low load

When more flexible needles were used, the peak forces were smaller, but the needle displacements increased (Fig. 10, *d–e*). At the lowest stiffness used (0.09 pN nm^{-1}), the force spikes were sharp and continuous rather than completely separated at 27°C (data not shown). Therefore, the temperature was decreased from 27 to 21°C to see more noticeably separated spikes (Fig. 10 *e*). We scored force or displacement spikes according to the same criteria as at high load. Fig. 12 *a* shows the PDS of signals (displacement spikes) without passing through a low-pass filter. The signals were in the frequency range from 1 to 50 Hz, so that the outputs were first passed through a low-pass filter with a bandwidth of 50 Hz (Fig. 10 *e*). The PDS approximately fitted the Lorentzian curve with a corner frequency of 7 Hz. We scored displacement spikes with durations larger than 12 ms (corresponding frequency = 14 Hz) and omitted the small spikes with amplitudes within 5 nm. Fig. 12 *b* shows the histogram of peak values of needle displacements. The histogram shows an approximately single broad Gaussian, with the maximum at 17 nm and the width at the half-maximum of 14 nm. The broadness in the figure, however, is apparent. To get the variance of displacements, the ran-

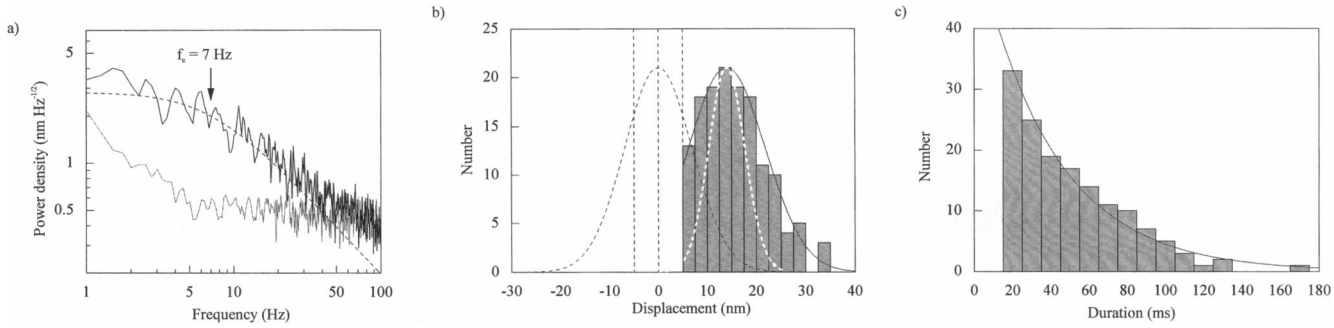

FIGURE 12 (*a*) PDS of displacement spikes at low load shown in Fig. 10 *e*. The lower trace indicates that of thermal vibrations of a free needle. (*b*) Histogram of the peak values of displacement spikes at low load. The force spikes were scored according to the criteria shown in text. Solid, broken, and dotted lines indicate the best fit Gaussian to displacement distribution, the Gaussian distribution of thermal vibrations of the needle when displacement spikes are not observed, and the subtracted Gaussian, respectively (see Discussion). Displacement spikes of which heights were within 5 nm were not scored (see text). (*c*) Histogram of the durations of the force spikes directly measured. A solid line indicates an exponential curve to fit over the histogram (τ = 40 ms).

domizing effect by the thermal vibration of the needle should be considered (see Discussion).

The mean durations of displacement spikes and zero-displacement periods directly measured as above were, respectively, 40 ms (k_- = 25 s^{-1}, Fig. 12 *c*) and 50 ms (k_+ = 20 s^{-1}), in good agreement with the corner frequency, 7 Hz, of the PDS as at high load. The average duration of displacement spikes, 40 ms, is more than two-fold larger than that reported by Finer et al. (1995) (15 ms at 17°C). This is probably because the stiffness of the needle used here is several times larger than their laser trap stiffness. Fig. 13 shows the relationship between the peak values of force spikes and the needle displacements measured by needles with varying stiffness.

DISCUSSION

Piconewton force and nanometer displacement measurements

We described an instrument that is able to measure the displacement of a fine glass needle attached to the actin filament at a nanometer resolution. The static position of the needle cannot be determined at a space resolution of less than approximately one-half of the wavelength of light due to the diffraction limit. Displacement, however, can be measured with greater accuracy (refer to Yanagida et al., 1993). As shown in this work, if the image of the needle is projected onto a pair of photodiodes and the displacement is determined by measuring the difference in the photocurrents of the photodiodes, a displacement of less than 1/1000 of the wavelength can be detected. This method is also used in an atomic force microscope to determine the position of the probe. Alternatively, an optical laser differential interferometer can be used (Denk and Webb, 1990; Svoboda et al., 1993; Svoboda and Block, 1994). A key point in constructing the instrument successfully is how to reduce the instrumental (mechanical, electric, and photon) noise, especially in the low frequency range (<50 Hz). We have used near infrared (700–900 nm) light from a halogen lamp for illuminating a needle. The light intensity of a halogen was very stable but was not high, so that the dark-current noise from photocurrent-voltage convert amplifiers was relatively large. Alternatively, a laser can be used. As laser intensity is very high, it could be used both to see fluorescent actin filaments and to illuminate the needle (Fig. 1 *b*, lower). As the laser is monochromatic and coherent, however, the problem is how to minimize inhomogeneity of illumination due to interference. For this purpose, a single-mode optical guide is often used. However, the interference pattern could not be completely eliminated. Furthermore, the differential output signals fluctuate considerably at low frequencies (<10 Hz), probably due to mechanical and thermal vibrations of the optical guide. Therefore, we abandoned the optical guide and simply put two lenses between the laser and a dichroic mirror to defocus the interference patterns (Fig. 1 *b*). This way, interference patterns were almost completely eliminated and the instrumental noise was greatly decreased (Figs. 2 *b* and 3 *b*). The instrumental noise at >1 Hz was much lower than that when a halogen lamp was used (Fig. 2, *a–d*) and was also lower than those

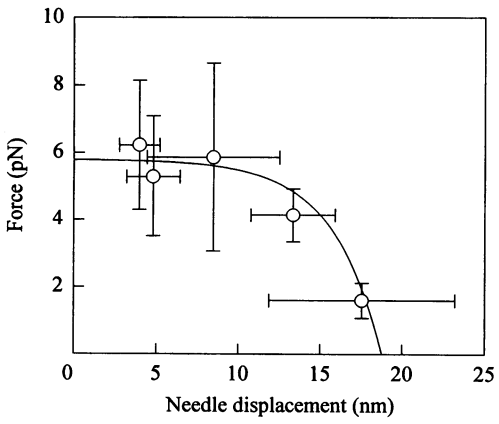

FIGURE 13 The relationship between peak values of force spikes and the needle displacements measured by needles with various stiffness. Bars indicate SD for 30–68 spikes.

reported by other investigators (Denk and Webb, 1990; Svoboda et al., 1993), but fairly large fluctuations of intensity still remained at <1 Hz. Therefore, the laser illumination system is useful to record relatively fast events at the present stage. It is noteworthy to mention that, although the system can detect the displacement of the needle with high space and time resolutions, the accuracy of the force and movement measurements produced by actomyosin motors is limited by thermal fluctuations of the needle. The rms error in a force measurement based on a single recording is given as $\sqrt{\langle \Delta F^2 \rangle_{error}} = \sqrt{(k_B TK)}$, where K is the stiffness of the needle, k_B the Boltzmann constant, and T the absolute temperature (refer to Kittel, 1958). The rms error in a displacement measurement is given as $\sqrt{\langle \Delta x^2 \rangle_{error}} = \sqrt{(k_B TK^{-1})}$. The value of $(\sqrt{\langle \Delta F^2 \rangle_{error}}) \times (\sqrt{\langle \Delta x^2 \rangle_{error}})$ cannot be smaller than $k_B T = 4$ pN nm; therefore, in principle, it is impossible to achieve a greater accuracy of simultaneous force and displacement measurements based on a single recording. If we sacrifice the time resolution, however, the accuracy of the measurements can be improved by decreasing Brownian noise by passing signals through a low-pass filter (Kittel, 1958).

One may be concerned that the Brownian force of a microneedle, which is much larger in size than protein molecules and undergoes large thermal vibrations, strongly interferes with the interaction of actomyosin when attached to the actin filament. However, even if more than two systems are connected, equilibrated to a big heat bath, thermal fluctuation of the composite system cannot exceed the amplitude determined by the equipartition law ($\frac{1}{2}k_B T$ in average energy per freedom; refer to Kittel, 1958). Namely, thermal fluctuation of the actomyosin motor is not amplified by being connected with the microneedle.

Forces from myosin molecules correctly oriented on a myosin rod cofilament

Using this instrument, we measured forces and displacements from multiple and single myosin heads in vitro. To avoid the effects of random orientation of myosin and association of myosin with an artificial surface, we used the filament assay instead of the surface assay. In this filament assay, the maximal velocity of actin sliding in the forward direction on the myosin filament at zero load was comparable to that in muscle (Fig. 8 *a*). The force per unit length of actin filament interacting with myosin was 36 and 52 pN μm^{-1} at myosin:rod ratios of, respectively, 1:1 and 2:1, at which the shape of filaments was similar to intact thick filaments (Table 1). As the force is approximately proportional to the content of myosin in the filaments at high myosin:rod ratios, the force on a pure myosin filament would be ~80 pN μm^{-1}. The force of the myosin head in a rabbit psoas muscle fiber was found to be 1.6 ± 0.2 pN, so the force per pair of thin and thick filaments is calculated as [(1.6 pN/head) × (420 heads/μm of thick filament)]/6 thin filaments = 112 pN per μm of thick filament interacting with a thin filament. This force is similar to that obtained in the in vitro filament assay. Thus, sliding velocity and force as large as in muscle are reproduced in vitro.

Force of individual heads determined from noise analysis of force fluctuations

The force of individual heads in the correct orientation estimated from the force fluctuations, 2.1 ± 0.4 pN, agrees with the average force (1.6 ± 0.2 pN) obtained by dividing the isometric force of a muscle fiber by the number of myosin heads contained within a half-sarcomere in cross-section. It has been widely believed that all myosin heads uniformly work and produce the same force in a muscle (Huxley, 1957). However, there has been no direct evidence for this basic hypothesis. The present results strongly support it. The force per head measured here, however, is approximately fivefold larger than that previously estimated in the myosin-coated surface assay, 0.4 pN (Ishijima et al., 1991). This is reasonable because, in the surface assay, the myosin molecules were randomly oriented, so that the force was the average of one of the heads interacting at various angles with actin filaments.

The duty ratio obtained here, 0.36, is somewhat smaller than that estimated from the stiffness (Goldman and Simmons; 1977; Higuchi and Goldman, 1991) or x-ray diffraction (Matsubara et al., 1975) of isometrically contracting muscle, ~0.8, but these values are not necessarily inconsistent with the present results because the duty ratio estimated from force fluctuations corresponds to time during which the myosin heads produce high force, whereas stiffness and x-ray diffraction estimate the total attached heads including weakly binding ones that produce small or zero force.

Stiffness

The stiffness measured by applying a sinusoidal length change with the frequency of 100 Hz was 0.024 pN nm^{-1}/pN force during force generation at high load. The stiffness increased linearly with the increase in the force and was extrapolated to zero at zero force. Therefore, the stiffness of the needle-to-myosin linkage is due mostly to actin-myosin interaction. As the maximal force of individual heads was approximately 6 pN (Table 2), the stiffness per head is estimated to be 0.14 pN nm^{-1}. But, this stiffness was that measured at a low frequency (100 Hz). As rapid rearrangement of actin-myosin attachment occurs to return to the original force level when length changes are applied to it (Huxley and Simmons, 1971), the stiffness should be larger at higher frequencies or in rigor. The stiffness at a low frequency (100 Hz) is approximately one-half of that at high frequencies of >500 Hz (Kawai and Brant, 1980) or that in rigor (Fig. 8 *c*). Therefore, the stiffness of actin-myosin interaction measured at high frequencies or in rigor would be approximately 0.28 pN nm^{-1}/head. Similar values have

been reported for single HMM molecules in the absence of ATP (0.3 pN nm^{-1}; Miyata et al., 1995) or at low ATP (0.13 pN nm^{-1}; Molloy et al., 1995a). These values are close to those of active (Huxley and Simmons, 1971) and rigor cross-bridges in muscle fiber (Tawada and Kimura, 1986).

Unitary forces and steps measured directly from single myosin heads

Unitary force

The relationship between the peak forces and the needle displacements when changing the stiffness of the needles was nonlinear (Fig. 13). This curve is reminiscent of the relation between the force and displacement in isometrically contracting muscle fibers following the quick recovery phase after sudden length changes, namely the T_2 curve (Huxley and Simmons, 1971). The force when extrapolated to zero displacement was approximately 6 pN, which is the peak force and not the force averaged over the whole ATPase cycle time. The averaged force, e.g., in the case of Fig. 10 *b*, is calculated as 6 pN $\times$ $(k_+ (k_+ + k_-)^{-1}) = 2$ pN. The peak and average force were compatible with those deduced from the force fluctuations (Table 2). As the transition rate out of the force generation state (k_-) was also compatible with that deduced from the force fluctuations (Table 2) as shown above, the kinetic characteristics of single myosin heads would be similar to those of individual heads when many heads work together.

The histogram of peak values of force spikes at high load shows a broad approximately Gaussian distribution (Fig. 11 *b*). The broad force distribution is probably due mostly to the randomizing effect by the thermal vibrations of the needle (Molloy et al., 1995b). When the needle is not sufficiently stiff, the actin filament attached to the needle would be longitudinally fluctuated by the thermal vibration of the needle. The myosin head would interact at some axial position of the actin filament and then produce displacement from that position. The displacement by the myosin head would thus be overlapped with the thermal vibration of the needle. Therefore, the variance of the peak forces should be obtained by subtracting the variance of the thermal vibration of the needle from it. In Fig. 11 *b*, a broken line indicates the Gaussian distribution of the thermal vibration of the needle when the actin filament does not interact with myosin in the forward region, and a solid line indicates the best fit Gaussian curve to the peak force distribution. The subtracted Gaussian curve, which is shown by a dotted line, gives the mean peak force of 5.8 pN and the standard deviation of 0.9 pN. Thus, the peak force would be rather constantly determined to be approximately 6 pN per head.

The peak force is considerably larger than those (2–4 pN on average) reported by Finer et al. (1994), Miyata et al. (1994), and Molloy et al. (1995a). This is, however, probably reasonable because, in their assays, HMM or S-1 molecules were randomly oriented on the surface, and some of the force spikes observed would be due to HMM or S-1 molecules that were not correctly oriented.

Unitary step

As mentioned above, to evaluate the displacement and the variance, the randomizing effect of the thermal vibrations of the needle should be considered (Molloy et al., 1995b). In Fig. 12 *b*, a dotted line indicates the Gaussian curve after subtracting the Gaussian distribution of the thermal vibration of the needle from that of displacement observed. The subtracted Gaussian curve gives the mean displacement of 17 nm and the standard deviation of 3.5 nm.

The mean needle displacement was obtained to be ~17 nm at low load (Fig. 12 *b*), but the needle displacement does not coincide with the displacement caused by the myosin head. Determining the displacement caused by the myosin head requires a correction for the needle-to-myosin linkage. The displacement caused by the head, d, can be obtained as $d = d_N (K_N + K_P) K_P^{-1}$, in which d_N is the needle displacement, K_N is the needle stiffness, and K_P is the linkage stiffness per head. Inserting $d_N = 17$ nm, $K_N = 0.09$ pN nm^{-1}, and $K_P = 0.28$ pN nm^{-1}/head, d is obtained tobe 23 nm.

If 23 nm is the length of a single power stroke, it is larger than that (14 nm) derived from quick release experiments on muscle fibers (Ford et al., 1977) and much larger than the most straightforward expectation (5–6 nm) from a shape change in the myosin head based on its atomic structure (Rayment et al., 1993) and based upon a small-angle x-ray scattering study (Wakabayashi et al., 1992). The large displacement observed here may be produced by multiple power strokes (Yanagida and Ishijima, 1995).

Other investigators have reported smaller mean values (10–15 nm; Finer et al., 1994; Miyata et al., 1994; Molloy et al., 1995a), but this difference would be also due to the effect of random orientation of myosin heads.

It is not clear how the single distinct displacement spikes correspond to ATP turnovers. Recently, we have developed new microscopy that enables us to directly visualize single fluorescent dye molecules in solution (Funatsu et al., 1995). This method can be extended to measure single mechanical events and ATP turnovers simultaneously. We will know how the myosin power strokes correspond to the ATP turnover in the near future.

APPENDIX

Noise analysis of force fluctuations based on a random on-off kinetic model

We consider that a myosin head occupies either the on state, in which the force is F_o, or the off (force = 0) stochastically. The autocorrelation

function of force fluctuations ($\delta F(t)$), which is deviation from mean force ($\langle F(t)\rangle$), i.e., $\delta F(t) = F(t) - \langle F(t)\rangle$, $\phi(\tau)$ is given as

$$\phi(\tau) = \langle \delta F(t) \times \delta F(t+\tau)\rangle = \langle F(t) \times F(t+\tau)\rangle - \langle F(t)\rangle^2$$

To calculate $\phi(\tau)$, we use the probability $p(\text{on}|t)$ that, given a head in the on state at time 0, the head is in the on state at time t. This probability is given by the following master equation:

$$\frac{1}{k}\cdot\frac{dp(\text{on}|t)}{dt} + p(\text{on}|t) = p_0$$

Here, $k = k_+ + k_-$, k_+ and k_- are rate constants of transitions into and out of the on state, respectively, and p_o is the probability that the head is in the on state in the steady state (Stevens, 1972). Solving this equation,

$$p(\text{on}|t) = (1 - p_0)e^{-k|\tau|} + p_0$$

Using $p(\text{on}|t)$,

$$\phi(\tau) = F_0^2(1 - p_0)p_0e^{-k|\tau|}$$

If N heads generate force independently, the autocorrelation function of force fluctuations caused by N heads, $\phi_N(\tau)$ is given by

$$\phi_N(\tau) = N F_0^2(1 - p_0)p_0e^{-k|\tau|}$$

The PDS, $\Phi_N(f)$ is given by taking the Fourier transform of $\phi_N(\tau)$ as

$$\Phi_N(f) = \frac{N F_0^2 p_0(1 - p_0)}{\pi f_c}\frac{1}{1 + (f/f_c)^2}$$

This PDS is called Lorentzian, in which the power density is constant at low frequencies and decreases with frequency squared (f^2) at high frequencies. The corner frequency, f_c, where $F_N(f)$ is one-half of the low frequency asymptote, gives k as $k = k_+ + k_- = 2\pi f_c$. The ATPase rate, V_{ATP} is given by $V_{ATP} = (k_+^{-1} + k_-^{-1})^{-1}$. Thus, k_+ and k_- are obtained by solving a quadratic equation for k_+ and k_-. p_o, i.e., the duty ratio, is given by $k_+ (k_+ + k_-)^{-1}$.

The mean squared force fluctuations, $\langle \delta F_N(t)^2\rangle$ is given by integrating $F_N(f)$ as

$$\langle \delta F_N(t)^2\rangle = N F_0^2 p_0(1 - p_0)$$

Rearranging this equation, we have

$$\frac{\sqrt{\langle \delta F_N(t)^2\rangle}}{\sqrt{\langle F_N\rangle}} = \sqrt{(1 - p_0)F_0}$$

Thus, if p_o is known, the slope of the plots of $\sqrt{\langle \delta F_N(t)^2\rangle}$ versus $\sqrt{\langle F_N\rangle}$ gives F_o. $\langle F\rangle$ is given by p_{oFo}.

We thank Y. E. Goldman (University of Pennsylvania), D. R. Vale (University of California, San Francisco), Y. Tanaka (HONDA R&D), Y. Nonomura (Tokyo University), and V. Lombardi (University of Florence) for valuable discussion. We thank Y. Okamoto (Obihiro University) for the gift of the antibody against myosin heavy chain.

REFERENCES

Bevington, P. R. 1969. Data Reduction and Error Analysis for the Physical Sciences. McGraw-Hill, New York. Chap. 5.

Burton, K. 1992. Myosin step size: estimates from motility assays and shortening muscle. *J. Muscle Res. Cell Motil.* 13:590–607.

Denk, W., and W. W. Webb. 1990. Optical measurement of picometer displacements of transparent microscopic objects. *Appl. Optics.* 29: 2382–2391.

Edman, K. A. 1979. The velocity of unloaded shortening and its relation to sarcomere length and isometric force in vertebrate muscle fibres. *J. Physiol.* 291:143–159.

Finer, J. T., A. D. Mehta, and J. A. Spudich. 1995. Characterization of single actin-myosin interactions. *Biophys. J.* 68:291s-297s.

Finer, J. T., R. M. Simmons, and J. A. Spudich. 1994. Single myosin mechanics: piconewton forces and nanometre steps. *Nature (Lond.).* 368:113–119.

Ford, L. E., A. F. Huxley, and R. M. Simmons. 1977. Tension responses to sudden length change in stimulated frog muscle fibres near slack length. *J. Physiol. (Lond).* 269:441–515.

Funatsu, T., Y. Harada, M. Tokunaga, K. Saito, and T. Yanagida. 1995. Imaging of single fluorescent molecules and individual ATP turnovers by single myosin molecules in aqueous solution. *Nature (Lond.).* 374: 555–559.

Goldman, Y. E., and R. M. Simmons. 1977. Active and rigor muscle stiffness. *J. Physiol.* 269:55–57

Hanson, J., and J. Lowy. 1963. The structure of F-actin and of actin filaments isolated from muscle. *J. Mol. Biol.* 6:46–60.

Harada, Y., A. Noguchi, A. Kishino, and T. Yanagida. 1987. Sliding movement of single actin filaments on one-headed myosin filaments. *Nature (Lond.).* 326:805–808.

Harada, Y., K. Sakurada, T. Aoki, D. D. Thomas, and T. Yanagida. 1990. Mechanochemical coupling in actomyosin energy transduction studied by in vitro movement assay. *J. Mol. Biol.* 216:49–68.

Higashi-Fujime, S. 1991. Reconstitution of active movement in vitro based on the actin-myosin interaction. *Int. Rev. Cytol.* 125:95–138.

Higuchi, H., and Y. E. Goldman. 1991. Sliding distance between actin and myosin filaments per ATP molecule hydrolysed in skinned muscle fibers. *Nature (Lond.).* 352:352–354.

Horiuti, K., T. Sakoda, and K. Yamada. 1993. Mechanical response to photolytic ATP pulsed of skinned muscle fibres pre-activated with a small pulse of ATP. *J. Muscle Res. Cell. Motil.* 14:335–340.

Howard, J., A. J., Hudspeth, and R. D. Vale. 1987. Movement of microtubules by single kinesin molecules. *Nature (Lond.).* 342:154–158.

Huxley, A. F. 1957. Muscle structure and theories of contraction. *Prog. Biophys. Biophys. Chem.* 7:255–318.

Huxley, A. F., and R. M. Simmons. 1971. Proposed mechanism of force generation in striated muscle. *Nature (Lond.).* 233:533–538.

Huxley, H. E. 1990. Sliding filaments and molecular motile systems. *J. Biol. Chem.* 265:8347–8350.

Ishijima, A., T. Doi, K. Sakurada, and T. Yanagida. 1991. Sub-piconewton force fluctuations of actomyosin in vitro. *Nature (Lond.).* 352:301–306.

Ishijima, A., Y. Harada, H. Kojima, T. Funatsu, H. Higuchi, and T. Yanagida. 1994. Single-molecule analysis of the actomyosin motor using nano-manipulation. *Biochem. Biophys. Res. Commun.* 199: 1057–1063.

Ishijima, A., and T. Yanagida. 1991. Force fluctuations on a single actin filament: interaction with oriented myosin molecules (Japanese). *Proc. 29th Japan Biophys. Sci. Meeting.* S195.

Itakura, S., H. Yamakawa, Y. Y. Toyoshima, A. Ishijima, T. Kojima, Y. Harada, T. Yanagida, T. Wakabayashi, and K. Sutoh. 1993. Force-generating domain of myosin motor. *Biochem. Biophys. Res. Commun.* 196:1504–1510.

Johara, M., Y. Y. Toyoshima, A. Ishijima, H. Kojima, T. Yanagida, and K. Sutoh. 1993. Charge-reversion mutagenesis of *Dictyostelium* actin to map the surface recognized by myosin during ATP-driven sliding motion. *Proc. Natl. Acad. Sci. USA.* 90:2127–2131.

Katz, B., and R. Miledi. 1971. Membrane noise produced by acetylcholine. *Nature.* 226:962–963.

Kawai, M, and P. W. Brant. 1980. Sinusoidal analysis: a high resolution method for correlating biochemical reactions with physiological processes in activated skeletal muscle of rabbit, frog and crayfish. *J. Muscle. Res. Cell Motil.* 1:279–303.

Kishino, A., and T. Yanagida. 1988. Force measurements by micromanipulation of a single actin filament by glass needles. *Nature (Lond.).* 334:74–76.

Kittel, C. 1958. Elementary Statistical Physics. J. Wiley and Sons, New York.

Kron, S. J., and J. A. Spudich. 1986. Fluorescent actin filaments move on myosin fixed to a glass surface. *Proc. Natl. Acad. Sci. USA.* 83: 6272–6276.

Lowey, S., G. S. Waller, and M. K. Trybus. 1993. Skeletal muscle myosin light chains are essential for physiological speeds of shortening. *Nature (Lond.).* 365:454–456.

Margossian, S. S., and S. Lowey. 1982. Preparation of myosin and its subfragments from rabbit skeletal muscle. *Methods Enzymol.* 85:55–71.

Matsubara, I., Y. E. Goldman, and R. M. Simmons. 1984. Changes in the lateral filament spacing of skinned muscle fibers when cross-bridges attach. *J. Mol. Biol.* 173:15–33.

Matsubara, I., N. Yagi, and H. Hashizume. 1975. Use of an x-ray television for diffraction of the frog striated muscle. *Nature (Lond.).* 255:728–729.

Miyata, H., H. Hakozaki, H. Yoshikawa, N. Suzuki, K. Kinoshita, Jr., T. Nishizaka, and S. Ishiwata. 1994. Stepwise motion of an actin filament over a small number of heavy meromyosin molecules is revealed in an in vitro motility assay. *J. Biochem.* 115:644–647.

Miyata, H., H. Yoshikawa, H. Hakozaki, N. Suzuki, T. Furuno, A. Ikegami, K. Kinoshita, Jr., T. Nishizaka, and S. Ishiwata. 1995. Mechanical measurements of single actomyosin motor force. *Biophys. J.* 286s-290s.

Molloy, J. E., J. E. Burns, J. C. Sparrow, R. T. Tregear, J. K. Jones, and D. C. S. White. 1995a. Single-molecule mechanics of heavy meromyosin and S1 interacting with rabbit or *Droshophila* actins using optical tweezers. *Biophys. J.* 298s-305s.

Molloy, J. E., J. E. Burns, J. C. Sparrow, and D. C. S. White. 1995b. Force and movement of myosin interacting with mutant actin, measured by optical tweezers. *J. Physiol.* In press.

Neher, E., and B. Sakmann. 1976. Single-channel currents recorded from membrane of denervated frog muscle fibres. *Nature (Lond.).* 260: 799–802.

Nishizaka, T., T. Yagi, Y. Tanaka, and S. Ishiwata. 1993. Right-handed rotation of an actin filament in an in vitro motile system. *Nature (Lond.).* 361:269–271.

Nonomura, Y. 1974. Fine structure of the thick filament in molluscan catch muscle. *J. Mol. Biol.* 88:445–455.

Prochniewicz, E., and T. Yanagida. 1990. Inhibition of sliding movement of F-actin by cross-linking emphasizes the role of F-actin structure in the mechanism of motility. *J. Mol. Biol.* 216:761–772.

Rayment, I., H. M. Holden, M. Whittaker, C. B. Yohn, M. Lorentz, K. C. Holmes, and R. A. Milligan. 1993. Structure of the actin-myosin complex and its implications for muscle contraction. *Science.* 261: 58–65.

Saitoh, K., T. Aoki, T. Aoki, and T. Yanagida. 1994. Movement of single myosin filaments and myosin step size on an actin filament suspended in solution by a laser trap. *Biophys. J.* 66:769–777.

Sellers, J. R., Y. J. Han, and B. Kachar. 1991. Movement of actin filaments by purified molluscan myosin and native thick filaments. *Biophys. J.* 59:187a.

Sellers, J. R., and B. Kachar. 1990. Polarity and velocity of sliding filaments: control of direction by actin and of speed by myosin. *Science.* 249:406–408.

Simmons, R. M., J. T. Finer, H. M. Warrick, B. Kralik, S. Chu, and J. A. Spudich. 1993. Force on single actin filaments in a motility assay measured with an optical trap. *In* Mechanism of Myofilament Sliding in Muscle Contraction H. Sugi and G. H. Pollack, editors. New York, Plenum Press. 331–336.

Stevens, C. F. 1972. Inferences about membrane properties from electrical noise measurements. *Biophys. J.* 12:1028–1047.

Sutoh, K., M. Ando, K. Sutoh, and Y. Y. Toyoshima. 1991. Site-directed mutations of *Dictyostelium* actin: disruption of a negative charge cluster at the N terminus. *Proc. Natl. Acad. Sci. USA.* 88:7711–7714.

Svoboda, K., and S. M. Block. 1993. Forces and velocities measured for single kinesin molecules. *Cell.* 77:773–784.

Svoboda, K., C. F. Schmidt, B. J. Schnapp, and S. M. Block. 1994. Direct observation of kinesin stepping by optical trapping interferometry. *Nature (Lond.).* 365:721–727.

Tawada, K., and M. Kimura. 1986. Stiffness of carbodiimide-crosslinked glycerinated muscle fibres in rigor and relaxing solutions at high salt concentrations. *J. Muscle Res. Cell Motil.* 7:339–350.

Toyoshima, Y. Y., S. J. Kron, E. M. McNally, K. R. Niebling, C. Toyoshima, and J. A. Spudich. 1987. Myosin subfragment-1 is sufficient to move actin filaments in vitro. *Nature (Lond.).* 328:536–539.

Toyoshima, Y. Y., S. J. Kron, and J. A. Spudich. 1990. The myosin step size: measurement of the unit displacement per ATP hydrolyzed in an in vitro assay. *Proc. Natl. Acad. Sci. USA.* 87:7130–7134.

Tregear R. T., and J. M. Squire. 1973. Myosin content and filament structure in smooth and striated muscle. *J. Mol. Biol* 77:279–290.

Uyeda, T. Q. P., S. J. Kron, and J. A. Spudich. 1990. Myosin step size estimation from slow sliding movement of actin over low densities of heavy meromyosin. *J. Mol. Biol.* 214:699–710.

Uyeda, T. Q. P., H. M. Warrick, S. J. Kron, and J. A. Spudich. 1991. Quantized velocities at low myosin densities in an in vitro motility assay. *Nature (Lond.).* 352:307–311.

Wakabayasi, K., M. Tokunaga, I. Kohno, Y. Sugimoto, T. Hamanaka, Y. Takezawa, T. Wakabayashi, and Y. Amemiya. 1992. Small-angle Synchrotron x-ray scattering reveals distinct shape changes of the myosin head during hydrolysis of ATP. *Science.* 258:443–447.

Weeds, A. G., and B. Pope. 1977. Studies on the chymotryptic digestion of myosin: effects of divalent cations on proteolytic susceptibility. *J. Mol. Biol.* 111:129–157.

Yamada, A., N. Ishii, and K. Takahashi. 1990. Direction and speed of actin filaments moving along thick filaments isolated from molluscan smooth muscle. *J. Biochem.* 108:341–343.

Yamada, A., and T. Wakabayashi. 1993. Movement of actin away from the center of reconstituted rabbit myosin filament is slower than in the opposite direction. *Biopys. J.* 64:565–569.

Yanagida, T. 1993. Myosin orientation-dependent force and step size. *Proc. 32nd Congr. Int. Union Physiol. Sci.* 10.

Yanagida, T., Y. Harada, and A. Ishijima. 1993. Nano-manipulation of actomyosin molecular motors in vitro: a new working principle. *Trends Biochem. Sci.* 18:319–324.

Yanagida, T., and Ishijima, A. 1995. Forces and steps generated by single myosin molecules. *Biophys. J.* 68:312s-320s.

Yanagida, T., M. Nakase, K. Nishiyama, and F. Oosawa. 1984. Direct observation of motion of single F-actin filaments in the presence of myosin. *Nature (Lond.).* 307:58–60.